This article has been accepted for inclusion in a future issue of this journal. Content is final as presented, with the exception of pagination.

Generic Approaches to Estimating Freeway Traffic State and Percentage of Connected Vehicles With Fixed and Mobile Sensing

Mingming Zhao, Claudio Roncoli, Yibing Wang, *Member, IEEE*, Nikolaos Bekiaris-Liberis, *Member, IEEE*, Jingqiu Guo, and Senlin Cheng

***Abstract*— Three filtering-based approaches to freeway traffic state estimation are studied using measurements from connected vehicles and also a minimum number of fixed detectors. These approaches are: *Method 1* based on EKF and the second-order traffic flow model METANET, *Methods 2* and 3 based on KF and the conservation equation that is driven by mean speed data of connected vehicles under a speed-uniformity assumption. Each method is capable of estimating segment traffic flow variables (speeds, densities, and flows) as well as segment market penetration rates (MPRs) of connected vehicles. The three methods are evaluated and compared in depth using NGSIM data with respect to their traffic state estimator design, data requirements, capabilities, limitations in the mixed sensing case. Recommendations are given about the choice of methods over the range of MPR.**

***Index Terms*— Freeway traffic state estimation, traffic flow modelling, connected vehicles, market penetration rate, mixed sensing, filtering, speed-uniformity assumption.**

I. Introduction

TRAFFIC state estimation (TSE) is essential for traffic surveillance and control. TSE aims at real-time inference of traffic flow variables on roadways with an adequate spatiotemporal resolution based on a limited amount of sensing data.

Manuscript received June 10, 2021; revised August 5, 2021; accepted September 15, 2021. This work was supported in part by the National Key Research and Development Program of China under Grant 2018YFB1600500 and Grant 2017YFE9134700, in part by the National Natural Science Foundation of China under Grant 71771200, and in part by the Provincial Key Research and Development Program of Zhejiang under Grant 2021C01012. The work of Claudio Roncoli was supported by the Academy of Finland Project Ubiquitous Localization, communication, and sensing infrastrucTuRe for Autonomous systems (ULTRA) under Grant 328216. The work of Nikolaos Bekiaris-Liberis was supported by the Hellenic Foundation for Research and Innovation (H.F.R.I.) under the "2nd Call for H.F.R.I. Research Projects to support Faculty Members and Researchers" under Project 3537/ORAMA. The work of Jingqiu Guo was supported by the Shanghai Social Science Planning Fund under Grant 2020JG008-BCK782. The Associate Editor for this article was Z. He. *(Corresponding authors: Yibing Wang; Jingqiu Guo.)*

Mingming Zhao and Yibing Wang are with the Institute of Intelligent Transportation Systems, Zhejiang University, Hangzhou 310058, China (e-mail: wangyibing@zju.edu.cn).

Claudio Roncoli is with the Department of Built Environment, Aalto University, 02150 Espoo, Finland (e-mail: claudio.roncoli@aalto.fi).

Nikolaos Bekiaris-Liberis is with the School of Electrical and Computer Engineering, Technical University of Crete, 73100 Chania, Greece (e-mail: bekiaris-liberis@ece.tuc.gr).

Jingqiu Guo is with the Key Laboratory of Road and Traffic Engineering of the Ministry of Education, Tongji University, Shanghai 201804, China (e-mail: guojingqiu@hotmail.com).

Senlin Cheng is with the School of Automation, Chongqing University, Chongqing 400044, China (e-mail: csl@cqu.edu.cn).

Digital Object Identifier 10.1109/TITS.2021.3121181

TSE used to be performed using sensing data from spot sensors (e.g. loops, radars, cameras) [1]–[6]. Nowadays, enabled by V2X communication capabilities, connected vehicles (CVs) can act as floating or mobile sensors to report in real time their own positions, speeds, and accelerations as well as their neighboring traffic state information, providing unprecedented opportunities for significantly improved TSE. The market penetration rate (MPR) of CVs is currently very low, and hence fixed-sensing and mobile-sensing technologies are expected to be used together for traffic surveillance and control in many years to come, thus highlighting the importance of TSE with mixed sensing. This paper addresses freeway TSE using mixed sensing data.

A. State-of-the-Art

According to [7], freeway TSE works are classified into three categories: model based, data based, and streaming data based. This paper focuses on the model-based TSE. In this category, typically the works are differentiated by traffic flow models employed for the estimator design and by filtering algorithms utilized.

A number of works have studied real-time freeway TSE with mixed sensing data based on the first-order Lighthill–Whitham–Richards (LWR) model or cell transmission model (CTM) model, using filtering techniques such as Kalman filter (KF) [8]–[10], extended Kalman filter (EKF) [11], [12], ensemble Kalman filter (EnKF) [13], [14], particle filters (PF) [15], [16], and heuristic smoothing algorithms [17], [18]. In order to better reproduce traffic phenomena such as capacity drop, scattering, hysteresis effect, stop-and-go waves, higher-order models have also been considered, such as the Payne-Whitham (PW) model [19], [20] and the Aw-Rascle-Zhang (ARZ) model [21], [22]. EKF was considered in [23], [24] to integrate mixed sensing data based on a PW-like model, while EKF and PF were applied respectively in [25], [26] based on the ARZ model. Recent overviews on freeway TSE using mixed sensing data are found in [7], [27].

Besides the works based on the first-order and higher order traffic flow models, an alternative approach to freeway TSE with mixed sensing data was recently developed by one research group [9], [10], [28]–[30]. The approach relies on an assumption that the average speed of regular vehicles in a road section is equal to that of CVs within the same road section.

TABLE I
TRAFFIC STATE ESTIMATION METHODS

Method 1	A TSE method based on METANET and EKF
Method 2	A TSE method based on speed-uniformity assumption and KF
Method 3	A TSE method based on MPR dynamics and KF

This speed-uniformity assumption is logical [10], [26], and has been validated with real data [8]. Following such assumption, instead of employing a non-linear traffic flow model as in the works mentioned above, a simplified model that considers only a "data-driven" conservation equation can be utilized for the traffic state estimator design, where a KF is applied to TSE.

In addition, despite a very significant task in the era of CVs, to our best knowledge, only two works [10], [26] have studied real-time estimation of MPR for connected/automated vehicles on freeways.[1] Firstly, again based on the speed-uniformity assumption, [10] derives a dynamic equation for MPR from the flow conservation equation of all vehicles and that of all CVs, provided that the density and flow of CVs are measurable for each freeway segment based on their regularly reported positions. KF is applied to the MPR estimation.

Exploiting the same speed-uniformity assumption, [26] establishes a connection between a two-class traffic flow model (for automated vehicles and human-driven vehicles) and a generalization of the ARZ model, then applying PF to estimate all traffic flow variables and MPR of automated vehicles. It was not explicitly stated what information is required of automated vehicles in order to deliver the MPR estimate.

B. This Work

Among the higher-order traffic flow models, the Payne-Whitham model [19], [20] was extended in [31] to deliver a second-order time-space-discretized traffic flow model METANET [32], which was shown to outperform a number of first-order models in some aspects [33]. Based on fixed sensing, METANET has been successfully applied with EKF to freeway TSE in simulation [1], [2], using real data [3]–[5], and for large-scale field applications [6]. So far, this METANET-EKF-based approach to freeway TSE has not been extended to the mixed sensing case, so it is unknown if the traffic state estimator so designed still keeps its capability and proper features demonstrated already in the fixed sensing case. This paper intends to address this issue, and refers to the METANET-EKF-based TSE approach as *Method 1*, see also Table I.

One alternative approach to freeway TSE [9, 10, 28-30] is to design a traffic state estimator based on a speed-uniformity assumption, which allows to formulate a model based on the vehicular conservation equation only, without resort to any speed equation. Consequently, the estimator design is largely simplified, leading to an easily implementable estimator. This approach is referred to as *Method 2* in this paper, see also Table I.

Yet another approach [10] first handles the MPR estimation for CVs on freeway, and further delivers the traffic state estimates for entire traffic flow using traffic measurements of CVs and MPR estimates. This approach is referred to as *Method 3* in this paper, see also Table I. In terms of direct MPR estimation for CVs, *Method 3* is so far unique in the literature of TSE. On the other hand, the MPR estimates could also be indirectly derived by *Methods 1* and *2*, but such a function of either *Method 1* or *2* was not investigated before. In any case, the study of the MPR estimation for freeway traffic (and also urban traffic) is much lacking.

Both *Methods 2* and *3* are novel also in that the involved dynamic systems can be formulated as linear parameter-varying ones by use of speed/flow/density measurements of CVs, and hence KF is sufficient for TSE. As reported in [37]–[40], among filtering algorithms, KF/EKF is the most efficient one in computation time, UKF's computation time may be of the same order as KF/EKF, but PF's and EnKF's computation times are much higher than KF/EKF's. Thus, PF and EnKF may have problems in real-time applications, while KF and EKF stand out in this aspect. *Methods 1-3* are all suitable for real-time applications.

Methodologically, the three methods represent different lines of thoughts, which are all generic and cover much of the "territory" of freeway TSE using mixed sensing data in the Eulerian scheme [27]. *Method 1* has not been applied to the mixed sensing case at all, and *Method 3* has only been studied so far in simulation with fictitious traffic data. Thus, it is highly interesting to further study their properties of traffic state and MPR estimation in the mixed sensing case, and also evaluate their performance with respect to the same test example of real data.

The major contributions of this paper are as follows:

(1) developing *Method 1* to incorporate mixed sensing data;
(2) developing two alternative approaches (in addition to *Method 3*) to real-time MPR estimation based on *Methods 1* and *2*;
(3) evaluating using NGSIM data *Methods 1-3* systematically for their traffic state estimator design, operating principles, data requirements, and capabilities for traffic state and MPR estimation as well as possible limitations, along with recommendations in consideration of the gradual increase of MPR.

The remainder of the paper is organized as follows. Section II formulates *Methods 1-3* along with their traffic

[1] A bit more studies on the same subject can be found for the urban case, typically relating to queue estimation at signalized intersections, see e.g. [34]–[36].

flow modeling and traffic state estimator design. Section III describes the evaluation setup and presents the evaluation results. Section IV presents further discussions. Section V concludes the paper.

II. Three Approaches to Freeway Traffic State Estimation

A. Mixed Sensing for Traffic State Estimation

Fixed sensors are able to provide complete information of passing vehicles at sensor locations, which, however, suffers from being local and sparse; while CVs as mobile sensors are advantageous in the spatial provision of speed information, but they cannot deliver accurate information of traffic volume and density, unless MPR reaches 100%.

1) Fixed Sensor Configuration: Flow observability of a road network refers to the capability that unmeasured traffic flows at the locations of no sensors can be inferred from measured traffic flows at locations with sensors. Flow observability is a pre-requisite for network traffic flow estimation. Unless the MPR of CVs is 100%, the flow observability of a road network depends on the configuration of fixed sensors.

A long freeway stretch is essentially a combination of a number of unit stretches, each with a pair of on/off-ramps. Given a unit stretch, there exist four configurations of fixed sensors, each securing the flow observability and hence allowing for TSE [2]. Since three methods are evaluated in this paper for TSE, without loss of generality and also for the ease of comparison and presentation, we stipulate that all three methods consider the same fixed sensor configuration for any unit stretch (Fig. 1), which includes three sensors in the freeway mainstream, at the upstream and downstream of the unit stretch, and also between the on/off-ramps (i.e. no sensor is installed at any on/off-ramp).

2) Fusion of Mixed Sensing Data: Following fluid mechanics, there are two schemes to formulate traffic flow modeling and model-based TSE: Eulerian and Lagrangian [27]. Accordingly, fixed (location-based) sensing and mobile (vehicle-based) sensing are also referred to as Eulerian and Lagrangian sensing, respectively. This paper addresses Eulerian traffic flow modeling and Eulerian TSE with mixed sensing data; in this case, the Lagrangian sensing data needs first to be converted into data in Eulerian coordinates and then used for TSE.

Specifically, the fundamental information from Lagrangian sensing data is regularly reported positions of CVs obtained via GPS or other similar systems. Based on this information, a number of "virtual" fixed sensors can be mimicked so as to deliver aggregated traffic flow data for TSE along with measurements from genuine fixed sensors.

B. Method 1 Based on METANET

For the formulation of all traffic flow models and TSE methods 1-3 reported in this paper, a common notation is employed, and summarized in Table II for the convenience of readers.

To facilitate the digital computation, spatiotemporal discretization is conducted with the following elements (see e.g. Fig. 1):

- a number N of segments, with segment length $\Delta_i, i = 1, 2, \ldots, N$;
- a number λ_i of lanes;
- a time step T and the discrete time indices $k = 0, 1, 2, \ldots$
- density $\rho_i(k)$ in veh/km/lane;
- space mean speed $v_i(k)$ in km/h;
- flow $q_i(k)$ in veh/h;
- on-ramp inflow $r_i(k)$ and off-ramp outflow $s_i(k)$, if any, in veh/h.

For segment i, the model equations are as follows:

$$\rho_i(k+1) = \rho_i(k) + \frac{T}{\Delta_i \times \lambda_i} \times \left[q_{i-1}(k) - q_i(k) + r_i(k) - s_i(k)\right], \quad (1)$$

$$q_i(k) = \lambda_i \rho_i(k) v_i(k) + \xi_i^q(k), \quad (2)$$

$$\begin{aligned} v_i(k+1) = {} & v_i(k) + \frac{T}{\tau}\left(V(\rho_i(k)) - v_i(k)\right) \\ & + \frac{T}{\Delta_i} v_i(k)\left[v_{i-1}(k) - v_i(k)\right] \\ & - \frac{\upsilon T\left[\rho_{i+1}(k) - \rho_i(k)\right]}{\tau \Delta_i (\rho_i(k) + \kappa)} \left(\frac{\delta T}{\Delta_i \times \lambda_i}\right) \\ & \times \left[\frac{r_i(k) v_i(k)}{(\rho_i(k) + \kappa)}\right] + \xi_i^v(k), \end{aligned} \quad (3)$$

$$V(\rho_i(k)) = v_f exp\left[-\frac{1}{a}\left(\frac{\rho_i(k)}{\rho_{cr}}\right)^a\right]. \quad (4)$$

Besides segment variables $\rho_1, \ldots, \rho_N, v_1, \ldots, v_N$, the model also includes model parameters v_f, ρ_{cr}, a, and boundary variables $q_0, v_0, \rho_{N+1}, r_{i_1}, \ldots, r_{i_m}, s_{i_1}, \ldots, s_{i_m}$, with i_1 and i_m denoting the indices of the first and last segments where on/off-ramps are present, assuming that on/off-ramps appear in pairs, $i_j \in \{1, 2, \ldots, N\}, j = 1, 2, \ldots, m, m \le N$. In addition, τ, υ, δ, and κ are constant parameters included in the dynamic speed equation (3), ξ_i^q and ξ_i^v denote modeling noise of flow and speed in segment *i*.

The dynamics of the model parameters and boundary variables are unknown; therefore, as introduced in [1]–[6], the random walk equation is applied to their modeling:

$$\theta(k+1) = \theta(k) + \gamma(k), \quad (5)$$

where θ addresses a model parameter or boundary variable to be modeled, and γ is a zero-mean Gaussian white noise. Thus, equations (1)-(5) can be written in a compact state-space form:

$$x_1(k+1) = f_1\left[x_1(k), \xi_1(k)\right], \quad (6)$$

where f_1 is a nonlinear vector function, x_1 refers to the state vector, and ξ_1 to the state noise vector, and

$$x_1 = \left[\rho_1, \ldots, \rho_N, v_1, \ldots, v_N, q_0, v_0, \rho_{N+1}, r_{i_1}, \ldots, r_{i_m}, s_{i_1}, \ldots, s_{i_m}, v_f, \rho_{cr}, a\right]^T, \quad (7)$$

$$\xi_1 = \left[\xi_1^q, \ldots, \xi_N^q, \xi_1^v, \ldots, \xi_N^v, \xi_0^q, \xi_0^v, \xi_{N+1}^\rho, \xi_{i_1}^r, \ldots, \xi_{i_m}^r, \xi_{i_1}^s, \ldots, \xi_{i_m}^s, \xi^{v_f}, \xi^{\rho_{cr}}, \xi^a\right], \quad (8)$$

TABLE II
NOMENCLATURE

State-space traffic flow models	
x	State vector
y	Output vector
f	Nonlinear vector function for state equation
g	Nonlinear vector function for output equation
ξ	State noise vector
η	Output noise vector
A_i	State matrix 1
B_i	State matrix 2
F_i	State matrix 3
C_i	Output matrix 1
G_i	Output matrix 2
Segment traffic flow variables in x	
ρ_i	Density of segment i
v_i	Mean speed of segment i
q_i	Flow of segment i
r_i	On-ramp inflow of segment i
s_i	Off-ramp outflow of segment i
Elements in y	
$m_0^q, m_N^q, m_{k_i}^q$	Flow measurements from fixed sensor in segment j (j =0, 1,2..., N)
$m_0^v, m_N^v, m_{k_i}^v$	Mean speed measurements from fixed sensor in segment j (j =0, 1,2..., N)
$m_{l_i}^v$	Mean speeds from CVs in segments l_i
Measurement of CVs	
v_i^c	Mean speed of CVs in segment i
ρ_i^c	Density of CVs in segment i
q_i^c	Flow of the CVs in segment i
r_i^c	Inflow of CVs at on-ramp of segment i
s_i^c	Outflow of CVs at off-ramp of segment i
p_i	Inverse of MPR of CVs in segment i
Traffic flow model parameters in f	
T	Model time step
Δ_i	Segment length of segment i
λ_i	Number of lanes of segment i
τ	Relaxation time
υ	Anticipation parameter
δ	Merging parameter
κ	Numerical stability parameter
V	Static speed-density relation
v_f	Free-flow speed
ρ_{cr}	Critical density
a	Exponent parameter

TABLE II
(Continued.) NOMENCLATURE

Elements in ξ	
ξ_i^q	Flow modeling noise of segment i
ξ_i^v	Mean speed modeling noise of segment i
ξ_0^q	Flow modeling noise at the upper bound of the freeway stretch
ξ_0^v	Mean speed modeling noise at the upper bound of the stretch
ξ_{N+1}^{ρ}	Density modeling noise downstream of the lower bound of the stretch
$\xi_{i_m}^r$	On-ramp flow modeling noise of segment i_m
$\xi_{i_m}^s$	Off-ramp flow modeling noise of segment i_m
ξ^{v_f}	Modeling noise of v_f
$\xi^{\rho_{cr}}$	Modeling noise of ρ_{cr}
ξ^a	Modeling noise of a
Elements in η	
$\eta_0^q, \eta_N^q, \eta_{k_m}^q$	Flow measurement noise of fixed sensors in segment j (j =0, 1,2..., N)
$\eta_0^v, \eta_N^v, \eta_{k_m}^v$	Mean speed measurement noise of fixed sensor in segment j (j =0, 1,2..., N)
$\eta_{l_i}^v$	Mean speed measurement noise from CVs in segments l_i

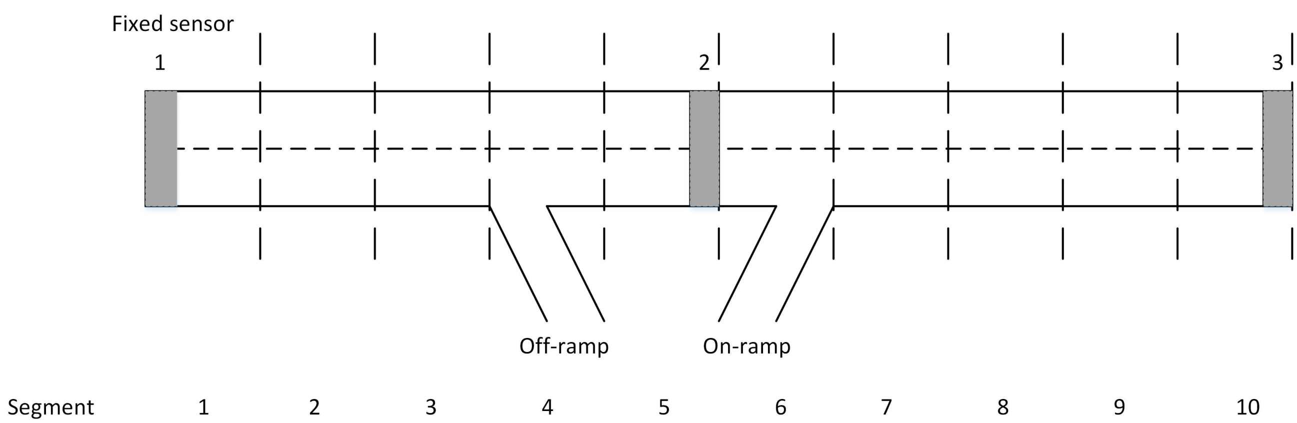

Fig. 1. A freeway stretch with 10 segments and 3 fixed sensors.

where ξ_i^q, ξ_i^v denote modeling noise of flow and mean speed at segment i, ξ_0^q, ξ_0^v denote modeling noise of flow and mean speed at the upper bounds of the freeway stretch, ξ_{N+1}^{ρ} denotes modeling noise of density right downstream of the lower bound of the stretch, $\xi^{v_f}, \xi^{\rho_{cr}}, \xi^a$ denote modeling noise of free speed, critical density and exponent parameter.

All involved traffic measurements may also be expressed in a state-space form:

$$y_1(k) = g_1\left[x_1(k), \xi_1(k), \eta_1(k)\right], \quad (9)$$

where y_1 is the output vector including all available traffic measurements, g_1 is a nonlinear vector function, and η_1 refers to the output (measurement) noise vector. More specifically,

$$y_1 = \left[m_0^q, m_0^v, m_N^q, m_N^v, m_{k_1}^q, m_{k_1}^v, \ldots, m_{k_m}^q, m_{k_m}^v, m_{l_1}^v, \ldots, m_{l_n}^v\right]^T, \quad (10)$$

$$\eta_1 = \left[\eta_0^q, \eta_0^v, \eta_N^q, \eta_N^v, \eta_{k_1}^q, \eta_{k_1}^v, \ldots, \eta_{k_m}^q, \eta_{k_m}^v, \eta_{l_1}^v, \ldots, \eta_{l_n}^v\right]^T. \quad (11)$$

(a) m_0^q, m_0^v, m_N^q, and m_N^v denote flow and mean speed measurements from fixed sensors at the upper and lower bounds of the freeway stretch, e.g. sensors 1 and 3 in Fig. 1.

(b) $m_{k_1}^q, m_{k_1}^v, \ldots, m_{k_m}^q, m_{k_m}^v$ denote the flow and mean speed measurements from the fixed sensors possibly installed in segments $k_1, \ldots, k_m$, $k_j \in \{2, \ldots, N-1\}, j = 1, 2, \ldots, m, m \le N-2$, for the purpose of flow observability, e.g. sensor 2 in Fig. 1.

(c) $m_{l_1}^v, \ldots, m_{l_n}^v$ denote mean speeds from CVs within segments $l_1, \ldots, l_n$, $l_j \in \{1, 2, \ldots, N\}, j = 1, 2, \ldots, n, n \le N$. When the MPR and measurement time interval are relatively high, CV data could be available from each segment at any time instant, i.e. $l_1 = 1$, $l_N = N$, e.g. from each segment in Fig. 1.

(d) η_1 denote the corresponding output noise in y_1.

Both aggregated flow and mean speed measurements from all fixed sensors are included in (10), while only aggregated mean speed measurements converted from speeds of all mobile sensors (individual CVs) are included in (10).

Concerning (b) and (c) above, if the mean speed information for a segment can be obtained via both a fixed sensor installed there and CVs, then the mean speed information from the former is used, because it covers all vehicles while that from the latter does not as long as the MPR is less than 100%. Equations (6) and (9) constitute a nonlinear dynamic system.

C. Method 2 Based on Speed-Uniformity Assumption

The speed-uniformity assumption states that, given a segment i, $v_i(k)$, the mean speed of all vehicles is equal to $v_i^c(k)$, the mean speed of all CVs in the segment. It is demonstrated in [10] that the mean of $v_i^c(k) - v_i(k)$ is close to zero even when MPR is very small, and the standard deviation of $v_i^c(k) - v_i(k)$ drops drastically and monotonically with the increase of MPR.

Consider MPR is not extremely low, then with segment mean speed $v_i(k)$ in (2) replaced by $v_i^c(k)$, we have:

$$q_i(k) = \lambda_i \rho_i(k) v_i^c(k) + \xi_i^q(k). \quad (12)$$

Substituting (12) into (1) leads to:

$$\begin{aligned}\rho_i(k+1) = \rho_i(k) + &\frac{T}{\Delta_i \times \lambda_i} \\ &\times \left[\lambda_{i-1}\rho_{i-1}(k) v_{i-1}^c(k) - \lambda_i \rho_i(k) v_i^c(k)\right] \\ &+ \frac{T}{\Delta_i \times \lambda_i} \times \left[r_i(k) - s_i(k) + \xi_{i-1}^q(k) - \xi_i^q(k)\right].\end{aligned} \quad (13)$$

In case of a very small MPR, it is possible that no CV could be present in a freeway segment over a certain time interval k, then the mean speed of CVs in the same segment over the last time interval $k-1$ is used instead, also with a default initial value set. It is again demonstrated in [10], [29] that the error so introduced to mean speed estimates is quite acceptable even with a small MPR and tends to be zero with the increase of MPR.

To model the unknown ramp flows, a random walk equation (5) is employed. Thus, equations (13) for all concerned freeway segments along with all random walk equations constitute a dynamic system of the state-space form:

$$x_2(k+1) = A_2\left(v^c(k)\right) x_2(k) + B_2 u_2(k) + F_2 \xi_2(k), \quad (14)$$

where

$$x_2 = [\rho_1, \ldots, \rho_N, r_{i_1}, \ldots, r_{i_m}, s_{i_1}, \ldots, s_{i_m}]^T, \quad (15)$$

$$u_2 = q_0, \quad (16)$$

$$\xi_2 = \left[\xi_1^q, \ldots, \xi_N^q, \xi_{i_1}^r, \ldots, \xi_{i_m}^r, \xi_{i_1}^s, \ldots, \xi_{i_m}^s\right]^T. \quad (17)$$

v^c is the vector of the mean speed of CVs in each segment, and ξ_2 stands for the noise in the random walk equations fixed sensor installed at the lower bound of the of on/off-ramp flows. Note that A_2 in (14) depends on v^c, while B_2 and F_2 are constant in relation to $\frac{T}{\Delta_i \times \lambda_i}$ ($i = 1, 2, \ldots, N$). Therefore, (14) is a linear parameter-varying system. All involved traffic measurements may also be expressed in a parameter-varying system form:

$$y_2(k) = C_2(v^c(k)) x_2(k) + \eta_2(k), \quad (18)$$

where

$$y_2 = [m_N^q, m_{k_1}^q, \ldots, m_{k_m}^q]^T, \quad (19)$$

$$\eta_2 = [\eta_N^q, \eta_{k_1}^q, \ldots, \eta_{k_m}^q]^T. \quad (20)$$

Like A_2 in (14), C_2 in (18) also depends on the real-time measurements of speeds of CVs. Unlike y_1 in (10), y_2 in (19) includes only flow measurements from fixed sensors. As aforementioned, *Methods 1-3* consider the same configuration of fixed sensors. Therefore, (19) and (10) share the same elements concerning flow measurements of fixed sensors. The interested reader is referred to [9], [10] for more details.

D. Method 3 Based on Dynamic Modeling for MPR

Following (1) for the dynamics of the total density, the dynamics of the density ρ_i^c of CVs reads:

$$\begin{aligned}\rho_i^c(k+1) = \rho_i^c(k) + \frac{T}{\Delta_i \times \lambda_i}&\left(q_{i-1}^c(k) - q_i^c(k)\right. \\ &\left. + r_i^c(k) - s_i^c(k)\right),\end{aligned} \quad (21)$$

where q_i^c is the flow of the CVs at segment i; r_i^c and s_i^c are the corresponding inflow and outflow of CVs at ramps. Let us define the inverse of MPR α_i of CVs at segment i as $\bar{p}_i$, i.e.,

$$\bar{p}_i(k) = \frac{\rho_i(k)}{\rho_i^c(k)} = \frac{1}{\alpha_i}. \quad (22)$$

And assume that the average speed of conventional vehicles in segment i equals the average speed of CVs in the same segment, we obtain $\bar{p}_i(k) = \frac{q_i(k)}{q_i^c(k)}$. Considering the inaccuracies introduced by the assumption, we have:

$$q_i(k) = \bar{p}_i(k) q_i^c(k) + \xi_i^q(k). \quad (23)$$

Thus, we get from (1), (21)–(23), formula (24), which is shown at the bottom of the next page, where $g_i^c(k)$ denotes the right-hand side of (21).

To model the unknown ramp flows, again a random walk (5) is employed. Thus, equations (24) for all concerned freeway segments along with all random walk equations constitute a linear parameter-varying dynamic system of the state-space form:

$$\begin{aligned}x_3(k+1) = &A_3\left(q^c(k), \rho^c(k), r^c(k), s^c(k)\right) x_3(k) \\ &+ B_3\left(q^c(k), \rho^c(k), r^c(k), s^c(k)\right) u_3(k) \\ &+ F_3\left(q^c(k), \rho^c(k), r^c(k), s^c(k)\right) \xi_3(k),\end{aligned} \quad (25)$$

where

$$x_3 = [\bar{p}_i, \ldots, \bar{p}_N, r_{i_1}, \ldots, r_{i_m}, s_{i_1}, \ldots, s_{i_m}]^T, \quad (26)$$

$$u_3 = q_0, \quad (27)$$

$$\xi_3 = [\xi_1^q, \ldots, \xi_N^q, \xi_{i_1}^r, \ldots, \xi_{i_m}^r, \xi_{i_1}^s, \ldots, \xi_{i_m}^s]^T, \quad (28)$$

where $q^c = \left[q_0^c \ldots q_N^c\right]^T, \rho^c = \left[\rho_0^c \ldots \rho_N^c\right]^T, r^c = \left[r_0^c \ldots r_N^c\right]^T, s^c = \left[s_0^c \ldots s_N^c\right]^T$.

Given a fixed sensor in segment i, the flow measurement m_i^q can be expressed by considering (23) as:

$$\begin{aligned} m_i^q(k) &= q_i(k) + \eta_i^q(k) \\ &= \bar{p}_i(k)\, q_i^c(k) + \xi_i^q(k) + \eta_i^q(k). \end{aligned} \quad (29)$$

Denote also by m_i^p the "measurement" of $\bar{p}_i$, then

$$m_i^p(k) = \frac{m_i^q(k)}{q_i^c(k)} = \bar{p}_i(k) + \frac{1}{q_i^c(k)}\xi_i^q(k) + \frac{1}{q_i^c(k)}\eta_i^q(k). \quad (30)$$

Thus, all involved traffic measurements may be expressed in a linear parameter-varying system form:

$$y_3(k) = C_3 x_3(k) + G_3\left(q^c(k)\right)\xi_3(k) + G_3(q^c(k))\eta_3(k), \quad (31)$$

where $y_3 = [m_N^p, m_{k_1}^p, \ldots, m_{k_m}^p]^T$, ξ_3 is already defined by (28), and $\eta_3 = [\eta_N^q, \eta_{k_1}^q, \ldots, \eta_{k_m}^q]^T$. The related mainstream flows $m_N^q(k)$ and $m_{k_i}^q(k)$, $i = 1, \ldots, m$, are available from fixed sensors in the corresponding segments, while q_N^c and $q_{k_i}^c$, $i = 1, \ldots, m$, are available from CVs. ξ_3 and η_3 are independent zero-mean Gaussian white, and their sum is still zero-mean Gaussian white. C_3 is a diagonal matrix with its non-zero elements all equal to one.

Note that in this case y_3 is related to both flow measurements from all fixed sensors and of all CVs passing the same locations. Flows q^c and densities ρ^c of all CVs in each segment as well as on/off-ramp flows of CVs are introduced to the state equation (25), while q^c is introduced to the output equation (31). The interested reader is referred to [10] for more details.

E. Traffic State Estimator Design

Consider the dynamic system formulations for the three methods, the traffic state estimator for *Method 1* can be designed on the basis of EKF as follows:

$$\begin{aligned} \hat{x}_1(k+1|k) = f_1\left[\hat{x}_1(k|k-1), 0\right] + K_1(k)\,[y_1(k) \\ -g_1\left(\hat{x}_1(k|k-1), 0\right)], \end{aligned} \quad (32)$$

where $\hat{x}_1(k+1|k)$ denotes the estimate of x at time instant $k+1$ based on measurements available until time instant k. The traffic state estimators for *Methods 2* and *3* can be designed on the basis of KF as follows:

$$\begin{aligned} \hat{x}_i(k+1|k) = A_i(k)\,\hat{x}_i\left((k|k-1) + B_i(k)\,u_i(k)\right. \\ +K_i(k)\,(y_i(k) - C_i\hat{x}_i(k|k-1)), \quad i = 2, 3. \end{aligned} \quad (33)$$

Note that the mean-speed measurement noise of CVs (e.g., due to speed information transmitted through a network) is not considered in (12) and (18) for *Method 2*, and similarly, the flow (and position) measurement noise of CVs is not considered in (23) and (29) for *Method 3*. It is not hard to extend the current formulations for *Methods 2* and *3* to address such measurement noise of CVs. However, the resulting systems would then incorporate noise terms that do not enter the process and measurement equations in an additive manner, and thus, a KF may not appear as a suitable choice anymore (rather, an EKF may be more appropriate). Nevertheless, as reported with the tests performed in [9], [10], [29], the current system formulations and estimator designs for *Methods 2* and *3* can tolerate the un-modeled non-additive measurement noise of CVs, which is consistent with the robustness properties of KF to non-additive noise reported in the literature, see e.g. [41].

F. Comparison of Three Estimators

The operational mechanisms of *Methods 1-3* are quite different; see Table III for a summary and Fig. 2 for comparison.

1) State Observability: In terms of fixed-sensing data, each method requires a minimum number of configuration of fixed sensors that respects the flow observability for the targeted freeway stretch/network [1], [2]. In terms of mobile-sensing data, both *Methods 1* and *2* exploit speed information of CVs, while *Method 3* requires flow and density information of CVs. Note that *Method 1* can work without mobile sensing data (as long as the flow observability is guaranteed by the fixed sensor configuration), while mobile sensing is indispensable for *Methods 2 and 3*. The state observability analysis in [10], [28] proves that the availability of mean speed information or the availability of flow and density information of CVs in each segment is essential for the state observability of *Method 2* or *Method 3*, as no dynamic model for average speed is employed.

2) Data Inputs: Any considered freeway stretch is spatially separated into a number of segments, and it is segment traffic flow variables like volumes, densities and mean speeds that are of interest to TSE. To take advantage of mobile sensing information for TSE, each method needs to be aware of the positions of CVs within the considered freeway stretch at any time so as to assign them to their corresponding segments in real time. Therefore, each method essentially needs the regularly reported position information of CVs, as stated in Section II-A-(2).

$$\bar{p}_i(k+1) = \frac{\left(\rho_i^c(k) - \frac{T}{\Delta_i}q_i^c(k)\right)p_i(k) + \frac{T}{\Delta_i}q_{i-1}^c(k)\,p_{i-1}(k) + \xi_{i-1}^q(k) - \xi_i^q(k)}{g_i^c(k)} + \frac{T}{\Delta_i}\frac{(r_i(k) - s_i(k))}{g_i^c(k)}, \quad (24)$$

TABLE III

COMPARISON OF METHODS *1-3* FOR FREEWAY TRAFFIC STATE ESTIMATION

				Method 1	***Method 2***	***Method 3***
Methodology	**Modeling**	Model		METANET (2^{nd}-order model)	Data-driven conservation equation	MPR dynamics derived from the data-driven conservation equation
		Mean speed dynamics based?		Yes	No	No
		Speed-uniformity assumption based (mean speed of regular vehicles is equal to that of CVs)?		No	Yes	Yes
		Ramp flow formulation		Random walk		
	Filtering	Algorithm		EKF	KF	KF
		OMPE considered?		Yes	No	No
	Sensing	Fixed	Flows needed?	Yes (ought to guarantee flow observability)		
			Mean speeds needed?	Yes	No	No
		Mobile	Indispensable?	No	Yes	Yes
			Aggregated data used	Segment mean speeds	Segment mean speeds	Segment densities and flows
			Way of usage	Output vector	State & output equations	State & output equations
TSE results	**Segment traffic flow variables**	Direct estimation		Segment speeds and densities	Segment densities	/
		Indirect calculation		Segment flows	Segment flows	Segment flows, densities, and speeds
	Segment MPRs	Direct estimation		/	/	Yes
		Indirect calculation		Yes	Yes	/
	Ramp flows	Direct estimation		Yes	Yes	Yes

Note that speeds of CVs may either be obtained by vehicle odometers or via trajectories of CV positions, while segment flows and densities of CVs can solely be obtained with trajectories of CV positions. Thus, in terms of measurement data input, *Methods 1* and *2* may potentially use more CV information than *Method 3*. This paper does not consider vehicle odometers, and hence all three methods are based on the same set of CV information.

3) Estimation Outputs: Method 1 delivers segment speed and density estimates simultaneously; *Method 2* presumes that the segment speeds are directly measurable via CVs, and focuses on segment density estimation; *Method 3* estimates MPR for each segment, from which we can compute a-posteriori segment flows and densities for all vehicles based on measured segment flows and densities of CVs, delivering segment speed estimates accordingly.

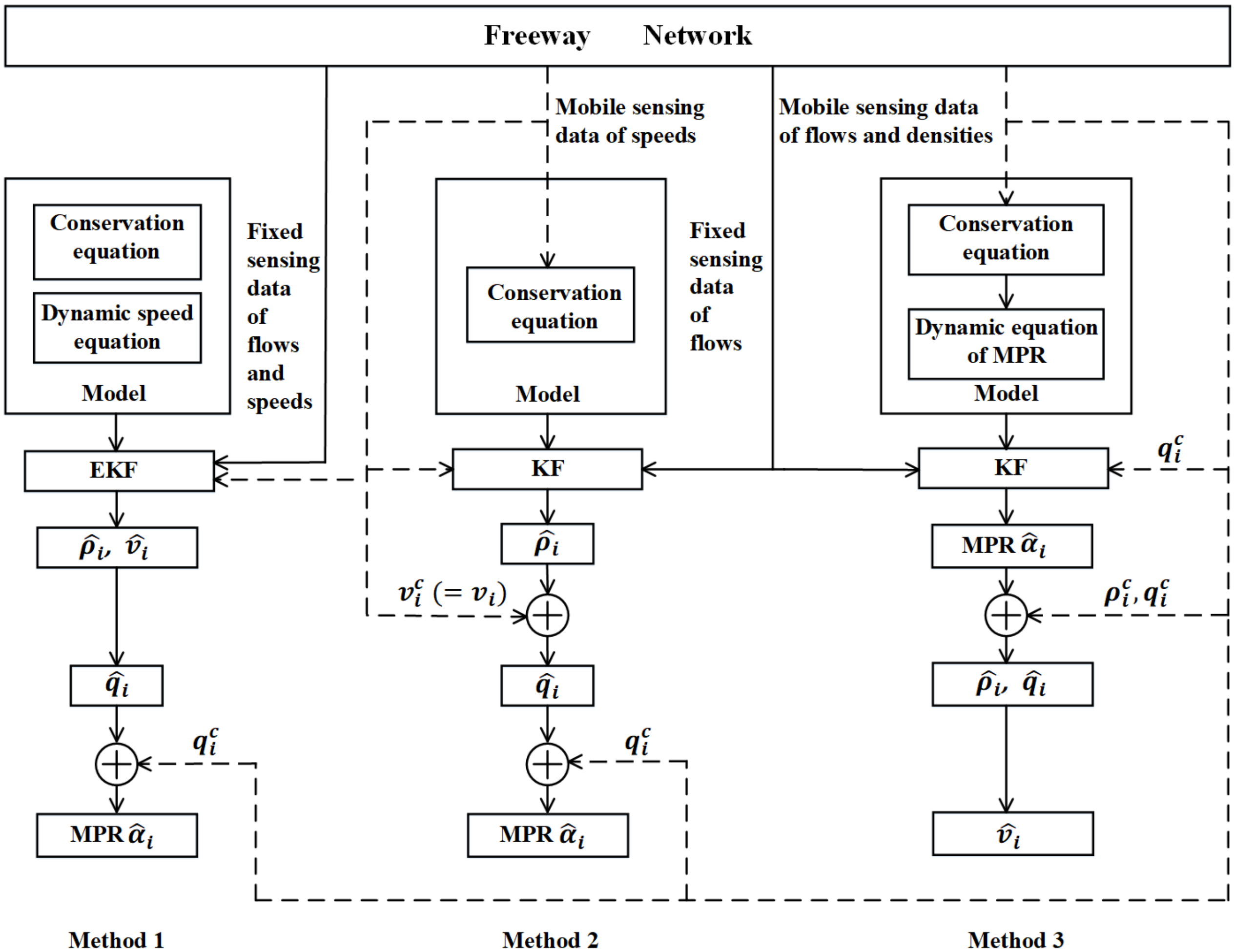

Fig. 2. Comparison of Methods 1-3. Any link from the freeway network to the model or EKF/KF represents an input, with a solid line for fixed sensing data and a dashed line for mobile sensing data; any link from EKF/KF represents an (estimated) output, denoted as $\hat{\omega}$ for a variable ω.

Note that *Methods 1* and *2* may also be applied to calculate MPR estimates once their segment flow or density estimates for all vehicles are computed. Therefore, each method can actually yield estimates for the same set of traffic state variables, and thus the three methods can be compared for their estimation performance.

More information of the three methods is found in Fig. 2 and Table III.

III. Evaluation Results

A. Evaluation Setup

Vehicle trajectory data from the Next Generation SIMulation (NGSIM) program was utilized in this work to evaluate the designed traffic state estimators. As shown in Fig. 3, the considered NGSIM highway stretch is composed of six lanes and includes one on-ramp close to its upstream end. The leftmost lane (Lane 1) was open only to high occupancy-vehicles (HOVs) presenting a clear bias in term of vehicle speeds, thus vehicle trajectory data collected from regular lanes (Lanes 2-6) was used for this work.

The considered data set was recorded from 4: 00 PM to 4: 15 PM on April 13, 2005. The original NGSIM data incorporates non-negligible errors in the positions of individual vehicles (see, e.g., [42]). Therefore, correction methodologies have been proposed in the literature to improve the data reliability, and the data used for this work was processed [43], [44].

For the purpose of macroscopic modeling and TSE, the stretch was divided into 4 segments, each of 100 meters in length, with the on-ramp located in segment 2. The model time step was set to be 5 s.

Regarding the fixed sensing conditions for this work, the original NGSIM highway stretch involved no fixed sensor, so the fixed sensing data employed was mimicked/converted from the available NGSIM vehicle trajectory data. With respect to the NGSIM highway stretch in Fig. 3, according to Section II-A, a pair of fixed sensors are needed at the upper and lower bounds of the stretch as illustrated in Fig. 3a for each method 1/2/3. *Method 1* is based on flow and speed measurements from fixed sensors 1 and 5 in Fig. 3a, while *Method 2*/3 requires only flow measurements from the same sensors.

The mobile sensing conditions is illustrated in Fig. 3b. *Method 1* accepts mean speed information of CVs in segments 1-3, *Method 2* requires mean speed information of CVs in

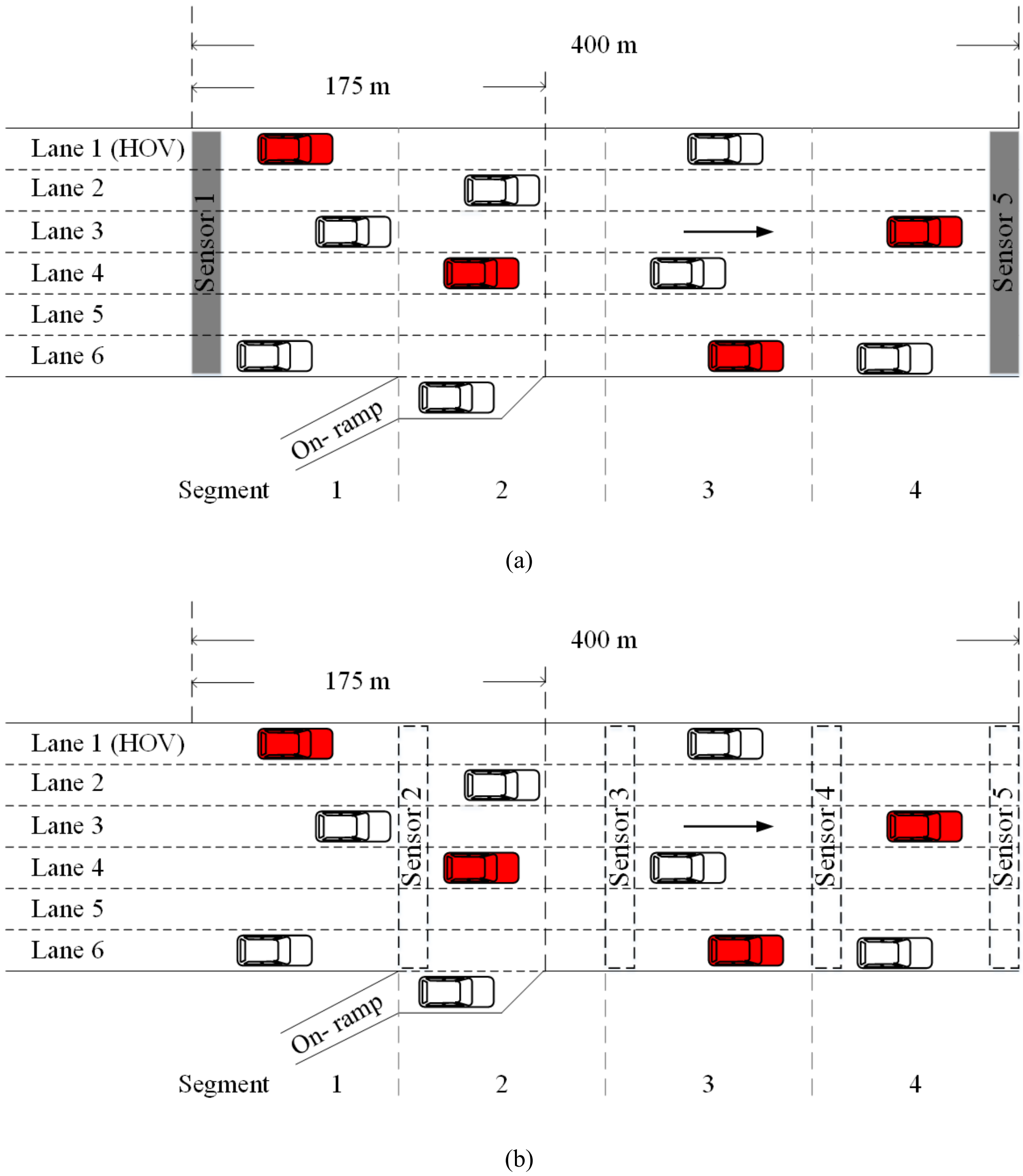

Fig. 3. A highway stretch of I-80 in Emeryville, California: (a) fixed sensor configuration; (b) mobile sensor configuration.

segments 1-4, *Method 3* requires flow and density information of CVs in segments 1-4. See also Table III.

The performance metrics considered are as follows:

$$RMSE = \sqrt{\frac{1}{KN}\sum_{k=1}^{K}\sum_{i=1}^{N}\left[x_i\left(k\right) - \hat{x}_i(k/k-1)\right]^2}, \tag{34}$$

$$MAPE = \frac{1}{KN}\sum_{k=1}^{K}\sum_{i=1}^{N}\frac{\left|x_i\left(k\right)-\hat{x}_i(k/k-1)\right|}{x_i(k)} \times 100\%, \tag{35}$$

$$BIAS = \frac{1}{K}\sum_{k=1}^{K}\left[x_i\left(k\right) - \hat{x}_i(k/k-1)\right], \tag{36}$$

$$NBIAS = \frac{\sum_{k=1}^{K}\left[x_i\left(k\right) - \hat{x}_i(k/k-1)\right]}{\sum_{k=1}^{K} x_i\left(k\right)}. \tag{37}$$

For this work, $N = 4$ (Fig. 3). The time horizon of the NGSIM data set is 15 minutes, and K in (34)-(37) is determined with setting the evaluation time interval set to be 30 s. As previously mentioned, the model time step is set to be 5 s. So, each evaluation time interval includes 6 model time steps, over which $\hat{x}_i(k|k-1)$ is delivered by each estimator 6 times, and what is eventually placed in (34)-(37) is the mean value of the six TSE values for every 30 s.

The three methods were evaluated and compared with (34) and (35) for their segment density, speed, and MPR estimates, and with (36) and (37) for their on-ramp flow estimates. With respect to the NGSIM data set used, the MPR is defined to be the sampled rate of vehicle trajectories in the data set.

Comprehensive evaluation results were obtained and are presented in Figs. 4-17. For the convenience of readers, the main contents of Figs. 4-17 are summarized in Table IV.

B. Density and Mean Speed Estimation

Figs. 4 and 5 depict the RMSE and MAPE results for *Methods 1-3* in terms of segment densities and speeds versus

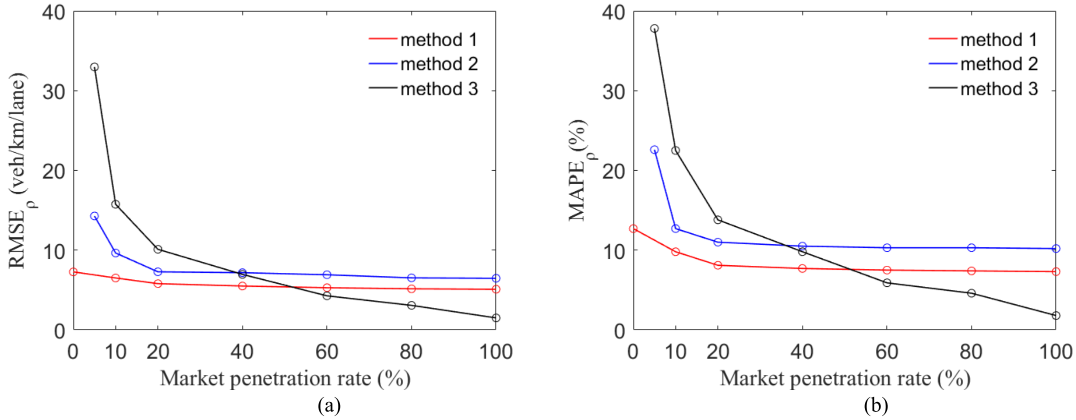

Fig. 4. The comparison of density estimation performance for the three methods: (a) RMSE; (b) MAPE.

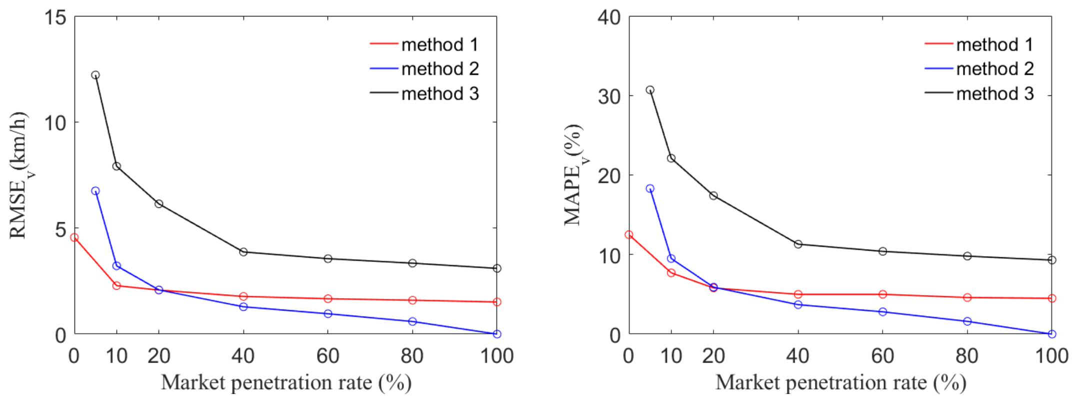

(a) (b)

Fig. 5. The comparison of speed estimation performance for the three methods: (a) RMSE; (b) MAPE.

the sampled MPR. Tables V and VI numerically compare the evaluation results for the three methods, when the sampled MPR ranges from 10% to 80%. The scenarios "Mixed-1" and "Mixed-2" in Tables V and VI are discussed in Section III-D. Figs. 6 and 7 depict the density and speed estimation results for segments 2 and 3 (in Fig. 3). Similar spot TSE results were also obtained for the other two segments (Fig. 3), but omitted for the sake of brevity.

Regarding the segment density estimation, it is noticed from Figs. 4a, 4b, Table V, and Fig. 6:

(1) the estimation errors reduce with the increase of the sampled MPR from 10% to 80% for each method;
(2) the estimation accuracy of *Methods 1* and *2* is moderately sensitive to MPR, while that of *Method 3* is significantly more sensitive;
(3) when MPR is lower than 40%, *Method 1* is more advantageous, while when MPR is larger than 60%, *Method 3* delivers the best results.

The speed estimation results are presented in Figs. 5a, 5b, Table VI, and Fig. 7. First, *Method 2* assumes that the mean speed of conventional vehicles is equal to that of CVs, and accordingly takes the mean speed of CVs in each segment as the segment speed estimate. With the increase of MPR, the speed estimate for each segment by *Method 2* approaches to the ground truth. That is why when MPR is equal to 100%, both RMSE and MAPE for the speed estimation by *Method 2* become zero in Figs. 5a and 5b. Overall, it is noticed from Figs. 5a, 5b, Table VI, and Fig. 7:

(4) the estimation accuracy of *Method 1-3* is sensitive to the increase of the sampled MPR;
(5) *Method 2* delivers the best speed estimates when MPR is bigger than 20%, which is not surprising as explained above.
(6) *Method 1* is quite more accurate than *Method 3* at each MPR.

Observations (1) and (4) above indicate that the usage of mobile sensing data is certainly beneficial for TSE. Observations (2) and (3) regarding the density estimation, and (5) and (6) regarding the speed estimation, can be further interpreted from the mechanisms of the three methods as follows.

Firstly, let us compare *Methods 1* and *2* for the density estimation. *Method 2* assumes the speed of any segment is

TABLE IV
FIGURES AND DESCRIPTIONS

Figure No.	Description
Basic Scenario of NGSIM	
4	RMSE and MAPE performance evaluation for **density estimates** in Methods 1-3 versus market penetration rate (MPR).
5	RMSE and MAPE performance evaluation for **speed estimates** in Methods 1-3 versus MPR.
6	**Density estimates** for segment 2 and 3 in Fig. 3 in TSE Methods 1, 2, and 3. The figure includes two columns and three rows. The left column addresses segment 2, and the right one addresses segment 3. The first, second, and third rows correspond to TSE Methods 1, 2, and 3. The legends in each plot refer to the real data and estimation results of various MPR values.
7	**Speed estimates** for segment 2 and 3 in Fig. 3. The figure is organized in exactly the same structure of Fig. 6.
8	**Flow estimates at the on-ramp** in Fig. 3 in TSE methods 1-3. The legends in each plot refer to the real data and estimation results of various MPR values.
9	It is the same as Fig. 8, but focuses on method 1 with a variety of MPRs. Fig. 8 is with a mild noise standard deviation (SD) for the ramp flow formulation, and Fig. 9 is with a bigger SD to check the tracking capability of ramp flow estimation.
10	**MPR estimates** in Method 3 for segment 2 and 3 in Fig. 3. The figure includes two columns and four rows. The left column addresses segment 2, and the right one addresses segment 3. The four rows correspond to the MPR values of 10%, 20%, 40%, 80%.
17	**Comparison of the MPR estimates** in Methods 1-3 versus MPR, with the results of Method 3 already presented in Fig. 10.
Compound Scenario over a Time Duration 2 Times Longer than the Basic Scenario	
11	**MPR estimates** in Method 3 for segment 2 and 3 in Fig. 3 based on **Compound scenario 1**.
12	**MPR estimates** in Method 3 for segment 2 and 3 in Fig. 3 based on **Compound scenario 2**.
13	**Density estimates** for segment 2 and 3 in Fig. 3, based on **Compound scenario 1** in Fig. 11 The legends in each plot refer to the real data and estimation results of Methods 1-3.
14	It is the same as Fig. 13, except it addresses **speed estimates**.
15 & 16	Same as Figs. 13 and 14, except that they address **Compound scenario 2** in Fig. 12.

TABLE V
PERFORMANCE OF DENSITY ESTIMATION

	RMSE (veh/km/lane)			**MAPE**		
Sampled MPR	*Method 1*	*Method 2*	*Method 3*	*Method 1*	*Method 2*	*Method 3*
10%	6.512	9.533	15.750	9.8%	12.7%	22.5%
20%	5.80	8.523	10.107	8.1%	11%	13.8%
40%	5.501	7.948	6.960	7.7%	10.5%	9.8%
60%	5.29	7.637	4.271	7.5%	10.3%	5.9%
80%	5.152	7.532	3.077	7.4%	10.3%	4.6%
Mixed-1 (10%-40%-20%)	5.743	8.745	13.648	8.7%	11.7%	17.2%
Mixed-2 (80%-40%-60%)	5.397	7.733	5.419	7.6%	10.4%	7.2%

directly measured with CVs, and is based on the conservation equation to estimates segment densities. In contrast, *Method 1* makes use of nearly the same amount of fixed and mobile sensing data, but it is based on a more sophisticated and also more thoughtful traffic flow model to deliver density and speed estimates simultaneously for any segment. Therefore,

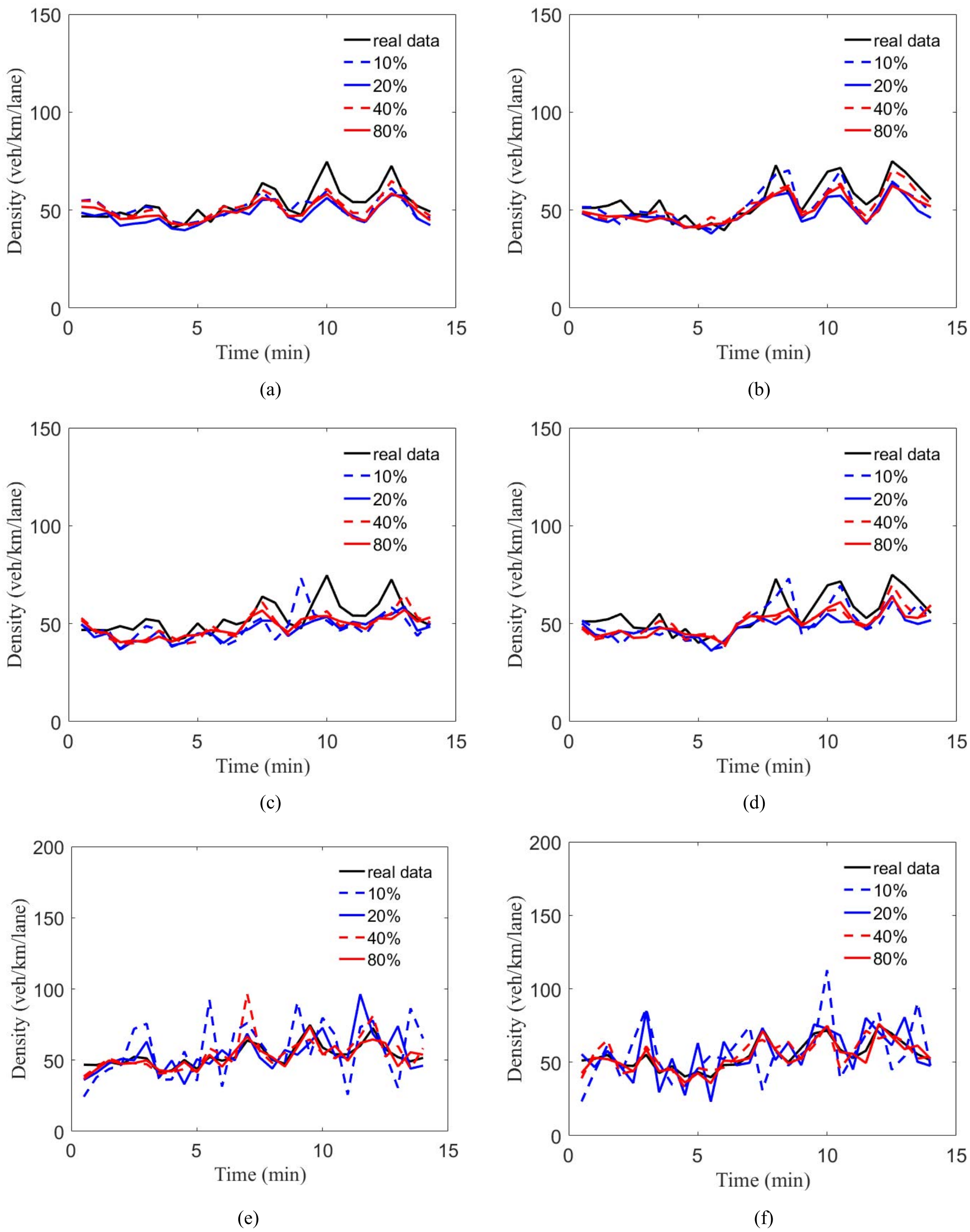

Fig. 6. Segment density estimates: (a), (b) Method 1; (c), (d) Method 2; (e), (f) Method 3; (a), (c), (e) segment 2; (b), (d), (f) segment 3 in Fig. 3.

the density estimation accuracy of *Method 1* is higher than that of *Method 2*.

Secondly, as previously explained, segment speeds are directly measured with *Method 2*. Therefore, it is not meaningful to compare *Methods 1* and *2* for the speed estimation.

Thirdly, let us compare *Methods 1* and *3* for the density estimation. Given a segment i, *Method 3* delivers the segment density (or flow) based on the density (or flow) of all CVs and the segment MPR estimate, i.e. $q_i\,(\mathrm{k}) = q_i^c\,(\mathrm{k})\,\bar{p}_i\,(\mathrm{k})$, $\rho_i\,(\mathrm{k}) = \rho_i^c\,(\mathrm{k})\,\bar{p}_i\,(\mathrm{k})$, see also Fig. 2. Both $q_i^c\,(\mathrm{k})$ and $\rho_i^c\,(\mathrm{k})$ involve measurement noise, and while calculating $q_i\,(\mathrm{k})$ and $\rho_i\,(\mathrm{k})$, the noise is amplified with $\bar{p}_i\,(\mathrm{k})$ (≥ 1) (see (22) in Section II-C). In general, the lower the MPR, the higher the errors for *Method 3* in estimating segment densities and flows. This is confirmed with Fig. 4, and Table V. Nevertheless, with the increase of MPR, *Method 3* eventually becomes superior to *Method 1* in the density estimation. This is probably because *Method 3* makes use of more connected vehicle information than *Method 1* (and *Method 2*), see Table III and Fig. 2.

Fourthly, let us compare *Methods 1* and *3* in term of speed estimation. Note that the segment speed estimates considered in Fig. 5 and in Table VI for *Method 3* were calculated

TABLE VI
PERFORMANCE OF SPEED ESTIMATION

	RMSE (km/h)			MAPE		
Sampled MPR	*Method 1*	*Method 2*	*Method 3*	*Method 1*	*Method 2*	*Method 3*
10%	2.283	3.219	7.912	7.7%	9.5%	22.1%
20%	2.076	2.082	6.138	5.8%	5.9%	17.4%
40%	1.776	1.288	3.871	5 %	3.7%	11.3%
60%	1.668	0.959	3.555	5%	2.8%	10.4%
80%	1.598	0.594	3.343	4.6%	1.6%	9.6%
Mixed-1 (10%-40%-20%)	1.89	2.156	6.267	5.4%	6.4%	17.4%
Mixed-2 (80%-40%-60%)	1.60	0.651	3.635	5.1%	2.7%	10.8%

as follows:

$$v_i(k) = \frac{q_i^c(k)}{\rho_i^c(k)}. \tag{38}$$

Since both q_i^c (k) and ρ_i^c (k) involve measurement noise, v_i (k) involves noise as well. That is probably why *Method 3* is inferior to *Method 1* in the speed estimation over the whole spectrum of MPR (Fig. 5, Table VI).

C. On-Ramp Flow Estimation

As shown in Fig. 3, the considered NGSIM highway stretch includes one on-ramp. The on-ramp flow estimation results are presented in Fig. 8 using the three methods. Note from Table III that the same random walk approach (see (5) in Section II-A) was applied in each method for the ramp flow estimation. It is seen from Fig. 8 that, with the MPR increase, the ramp flow estimates tend to approach the trend of the ramp flow curve for each method. The estimates are also evaluated using the criteria of BIAS and NBIAS in Table VII. The estimation accuracy increases with MPR. The scenarios "Mixed-1" and "Mixed-2" in Table VII are discussed in Section III-D.

Note that the results in Fig. 8 and Table VII (MPR = 10% - 80%) are obtained with a mild standard deviation (SD) for the noise in the random walk equation. With a bigger SD considered, however, a much quicker adaption of the estimation towards the ramp flow is observed in each method, see Fig. 9 for *Method 1*.

D. MPR Estimation

Only *Method 3* can directly deliver MPR estimates. This capability is demonstrated in this section using the same NGSIM data set. By sampling the trajectories of all NGSIM vehicles that consecutively entered the freeway stretch according to the percentage of 10%, 20%, 40%, and 80%, a number of vehicle trajectories were picked up to mimic those of CVs. The above percentages are referred to as the sampled MPR for this evaluation study. Because vehicle trajectories in the NGSIM data set are not evenly distributed in time and space, the resulting MPRs at the mainstream and on-ramp entries are not constant. Thus, the MPR in each segment is not constant, for any given sampled MPR, which is confirmed in Figs. 10-12 below. Fig. 10 display actual MPR values and their estimates in segments 2 and 3 in Fig. 3. Similar results were observed for segments 1 and 4 but omitted for brevity. Given a sampled MPR, the resulting segment MPRs fluctuate around the sampled MPR, and with the increase of the sampled MPR, the amplitudes of fluctuation are reduced. In any case, the MPR estimates tracked the actual MPRs in all segments quite well, and the higher the sampled MPR, the more accurate the estimates, see also Table VIII for *Method 3* (MPR = 10% - 80%).

Recall that the original NGSIM data set covers only 15 minutes. In order to further explore the dynamics of segment MPR and the tracking capability of the MPR estimator, a demand scenario of 45 minutes was created by replicating the original NGSIM data twice over the second and third periods of 15 minutes each. In addition, the sampled MPR over the first, second, and third periods were set to be 10%, 40%, and 20%. As displayed in Fig. 11, the segment MPRs were still estimated quite well, and in particular, the MPR estimator was able to closely track the sharp increase and decrease of MPR at the end of the first and second periods of 15 minutes; see also the last second line of Table VIII. Another test is presented in Fig. 12, with the sampled MPRs over the first, second, and third periods of 15 minutes set to be 80%, 40%, and 60%. Again, the MPR estimator was able to track the sharp changes of MPR quite satisfactorily; see also the last line of Table VIII.

To further demonstrate the estimation performance of the three methods, the estimates of segment densities and speeds for the MPR scenarios depicted in Figs. 11 and 12 are

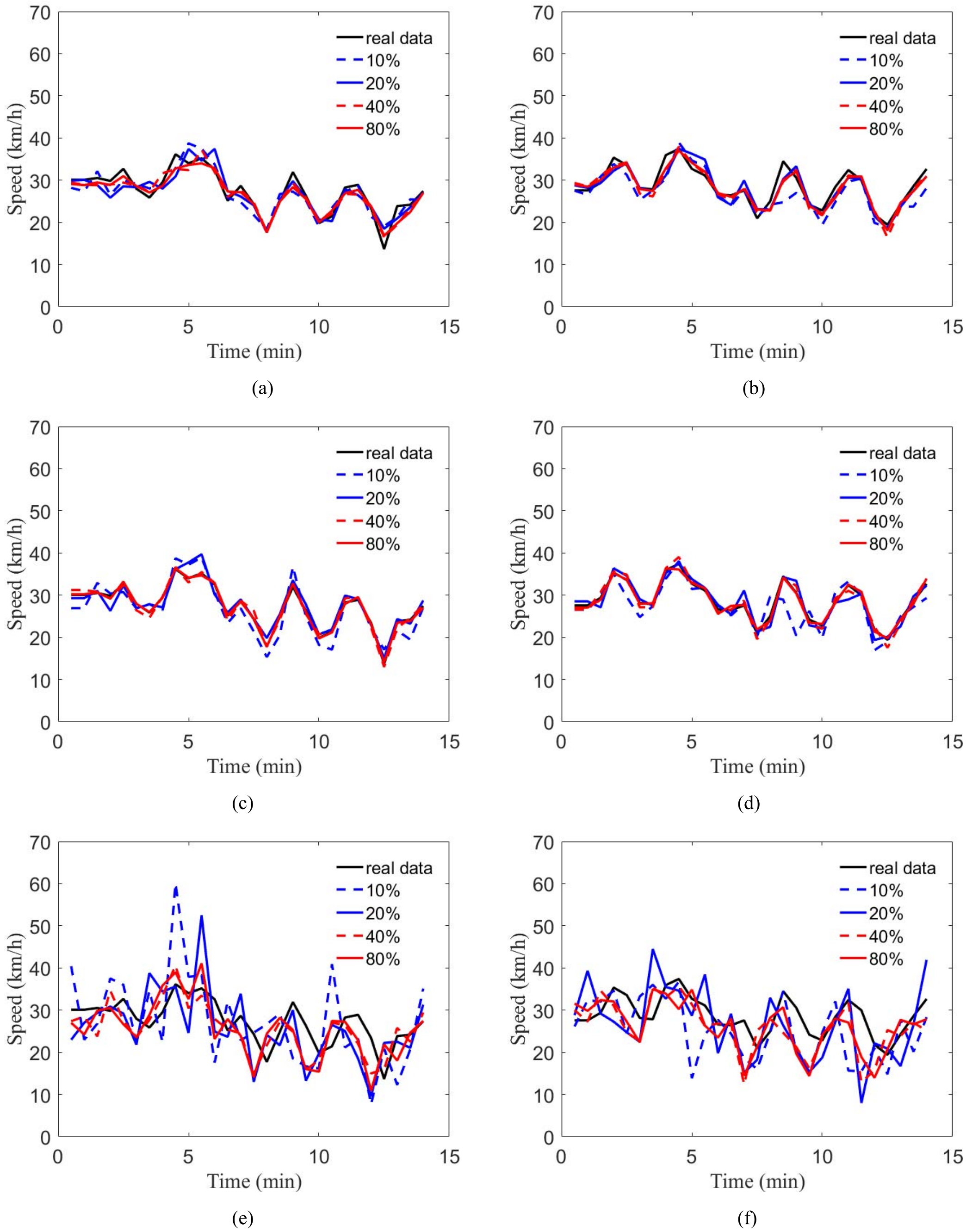

Fig. 7. Segment speed estimates: (a), (b) Method 1; (c), (d) Method 2; (e), (f) Method 3; (a), (c), (e) segment 2; (b), (d), (f) segment 3 in Fig. 3.

also evaluated, with the corresponding results presented in Figs. 13-16 as well as in the last two lines of Tables V–VIII.

Note that *Methods 1-3* utilize the same CVs measurements derived from the same NGSIM data. Once *Methods 1* and *2* obtain their segment density estimates for all vehicles, both methods can also deliver their respective MPR estimates for each segment. Fig. 17 and Table VIII compare the MPR estimation capability of the three methods, with the results of *Method 3* already presented in Fig. 10.

In contrast to Fig. 4a and Table V, the RMSE results for MPR estimates by *Method 1/2* in Fig. 17a and Table VIII increase with MPR. At first sight, this is surprising, but it could be explained as follows. Let ρ_i^c and ρ_i denote the density of CVs and that of all vehicles for a segment i. For either method, ρ_i^c is measurable, but ρ_i needs to be estimated, and let the estimate be $\hat{\rho}_i$. Let us denote also the segment MPR and its estimate by α_i and $\hat{\alpha}_i$. Then, $\hat{\alpha}_i - \alpha_i = \rho_i^c \left[\frac{1}{\hat{\rho}_i} - \frac{1}{\rho_i}\right]$. Note that $\left[\frac{1}{\hat{\rho}_i} - \frac{1}{\rho_i}\right]$ is little sensitive to MPR α_i for MPR lager than about 10% (see also Fig. 17b), but ρ_i^c is a monotonically increasing function of α_i. Thus, the increase of RMSE with MPR is attributed to a more aggressive increase of ρ_i^c with MPR, as compared to the change of $\frac{1}{\hat{\rho}_i} - \frac{1}{\rho_i}$ with MPR α_i, given that $\hat{\alpha}_i - \alpha_i$ is the dominant term in (34).

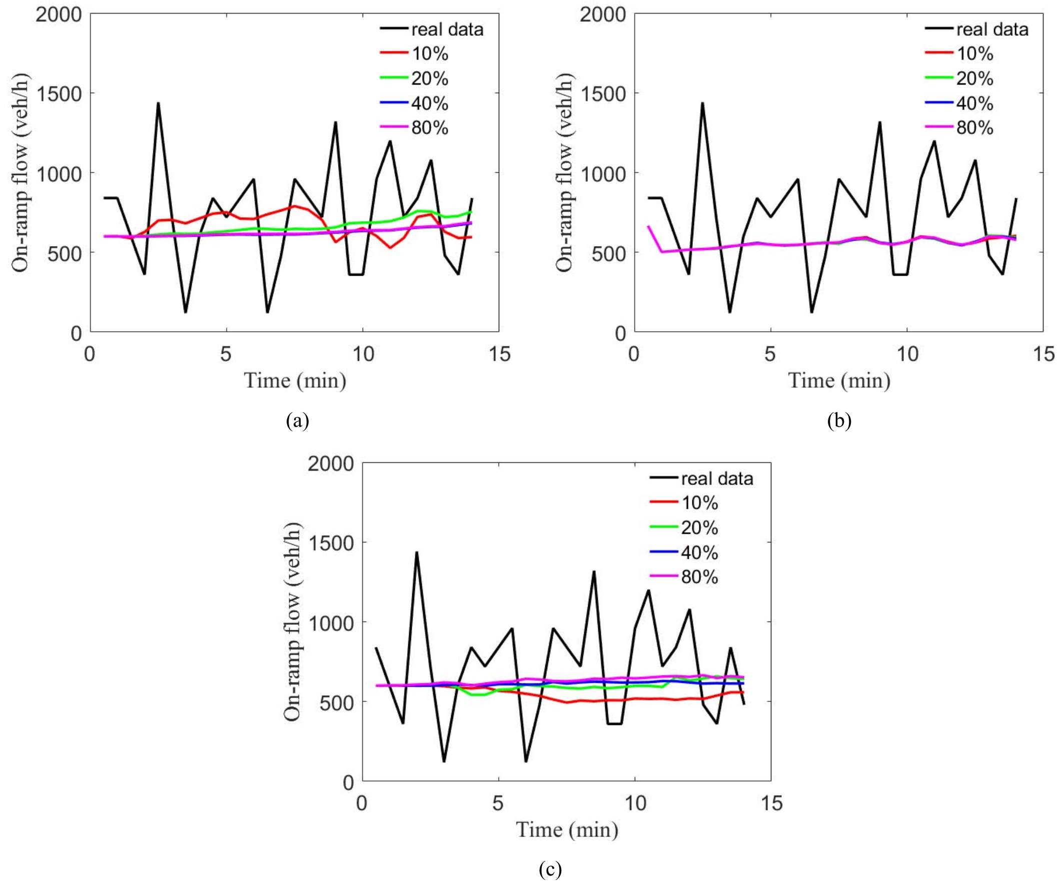

Fig. 8. On-ramp flow estimates based on (a) Method 1; (b) Method 2; (c) Method 3.

TABLE VII
PERFORMANCE OF ON-RAMP FLOW ESTIMATION

	BIAS (veh/h)			NBIAS		
MPR	*Method 1*	*Method 2*	*Method 3*	*Method 1*	*Method 2*	*Method 3*
10%	109.2	134.3	171.6	14.9%	18%	23.4%
20%	106.4	133.9	118.5	13.5%	17.9%	16.2%
40%	82.8	133.5	107.8	11.9 %	17.8%	14.7%
60%	80.1	133.2	93.7	11.2%	17.7%	12.6%
80%	7.3	133.1	87.6	10.8%	17.7%	11.9%
Mixed-1 (10%-40%-20%)	108.6	133.8	149.4	13.2%	17.9%	20.4%
Mixed-2 (80%-40%-60%)	81.2	133.3	95.8	11.4%	17.7%	13%

On the other hand, the MAPE results in Fig. 17b and Table VIII decrease with MPR. In fact, Fig. 17b and Table VIII for MPR are quite comparable to Fig. 4b and Table V for density. This is because the dominant factor of MAPE in (35) for MPR estimates of segment i is equal to: $\frac{\alpha_i - \hat{\alpha}_i}{\alpha_i} = \frac{\hat{\rho}_i - \rho_i}{\hat{\rho}_i}$, but the key item in the MAPE index (35) for density of segment i reads: $\frac{\rho_i - \hat{\rho}_i}{\rho_i}$. Therefore, Fig. 17b and Table VIII for MPR are highly relevant to Fig. 4b and Table V for density.

IV. DISCUSSIONS

A. Recommendations

The investigation results from this work show that no method outperforms the others in every aspect:

(1) *Method 2* delivers the best results of segment speeds when MPR is bigger than 20% (Fig. 5);

(2) *Method 3* delivers the best MPR and density estimates when MPR is bigger than 50% (Figs. 17b and 4b);

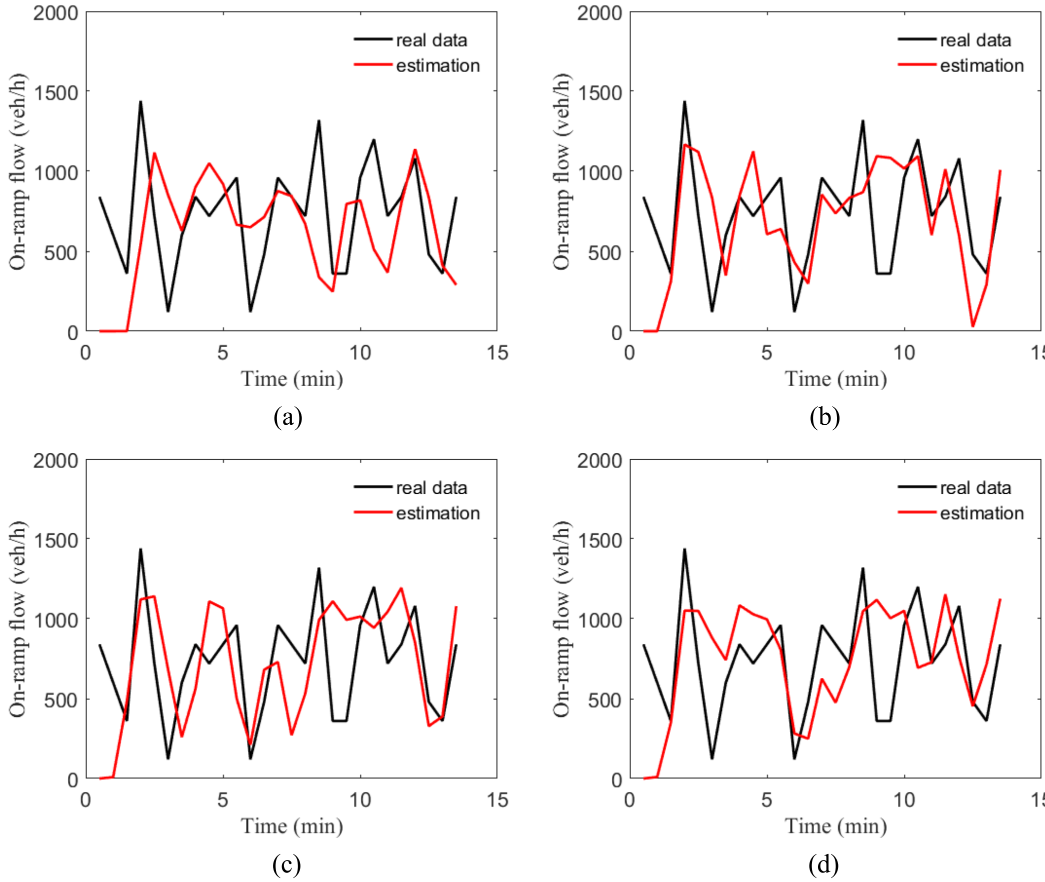

Fig. 9. On-ramp flow estimates based on Method 1 with MPR equal to (a) 10%, (b) 20%, (c) 40%, (d) 80%.

TABLE VIII
PERFORMANCE OF MPR ESTIMATION

	RMSE			MAPE		
MPR	*Method 1*	*Method 2*	*Method 3*	*Method 1*	*Method 2*	*Method 3*
10%	1.4%	2%	2.8%	10.5%	12.4%	29.7%
20%	2%	2.8%	3.4%	8.8%	11%	14.6%
40%	3.4%	4.9%	4.7%	7.8 %	10.4%	9.3%
60%	5.6%	7.7%	4.7%	7.7%	10.3%	6%
80%	8.6%	11.9%	4.6%	8.4%	12.3%	4.7%
Mixed-1 (10%-40%-20%)	6%	3.5%	4.3%	10.6%	11.2%	18.2%
Mixed-2 (80%-40%-60%)	5.7%	8.9%	5%	7.8%	10.4%	7.2%

(3) *Method 1* is more balanced on the density, speed, and MPR estimates.

Note again that *Method 1* can work without mobile sensing data, while *Methods 2* and *3* cannot. *Method 2* takes advantage of speeds of CVs in each segment, *Method 3* exploits the density and flow of CVs in each segment, all based on regularly reported positions for CVs.

In general, the following recommendations are given:

(1) when MPR is less than 10%, *Method 1* is recommended for all density, speed, and MPR estimation;

(2) when MPR is bigger than 20%, there is no benefit in calculating speed estimates, which can be obtained directly from CV measurements; in fact, we observe that speed errors in *Method 2* are smaller than in *Methods 1* and *3*.

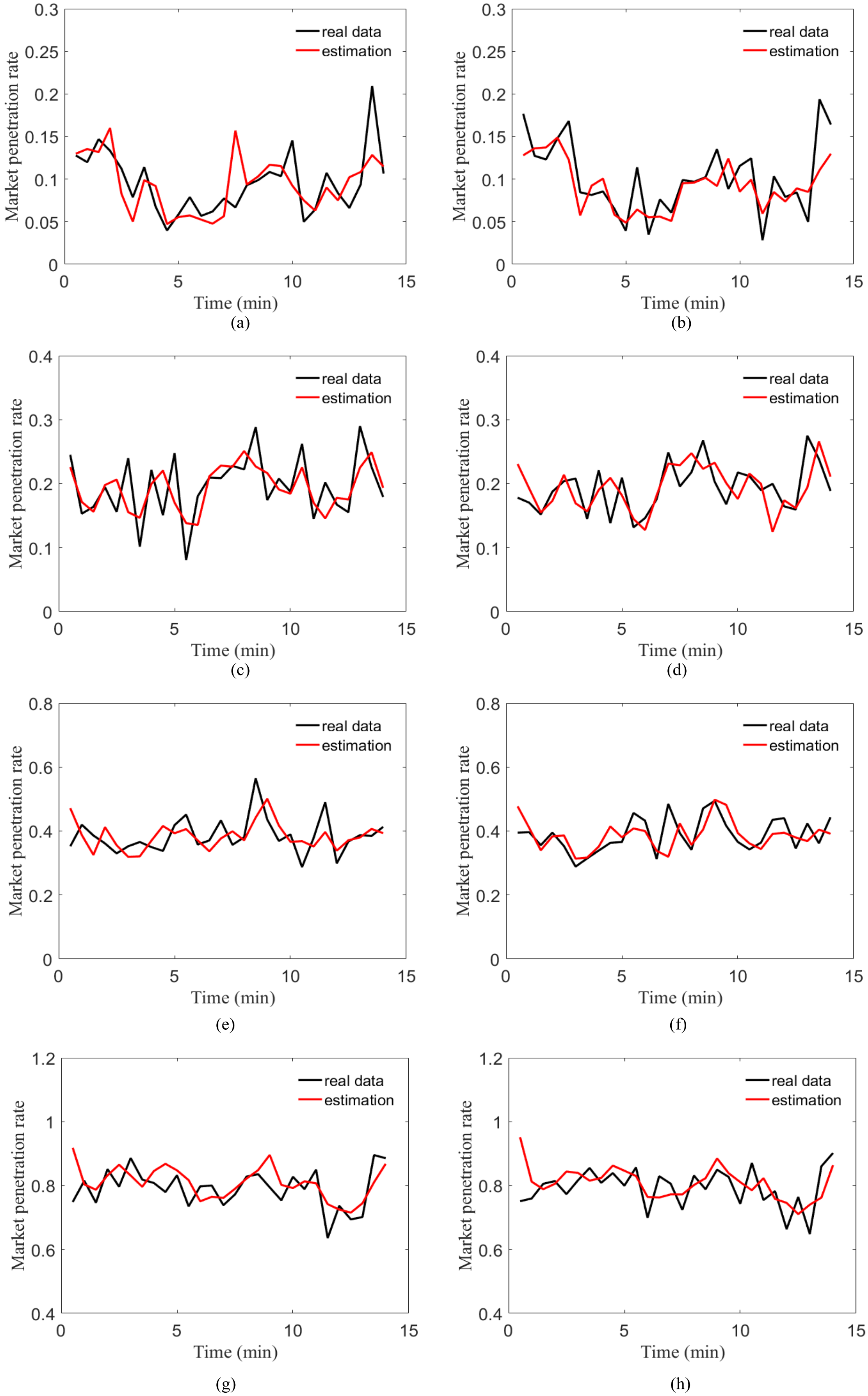

Fig. 10. MPR estimates in Method 3 for segments 2 and 3 in Fig. 3: (a), (b) MPR equal to 10%; (c), (d) MPR equal to 20%; (e), (f) MPR equal to 40%; (g), (h) MPR equal to 80%; (a), (c), (e), (g) segment 2; (b), (d), (f), (h) segment 3.

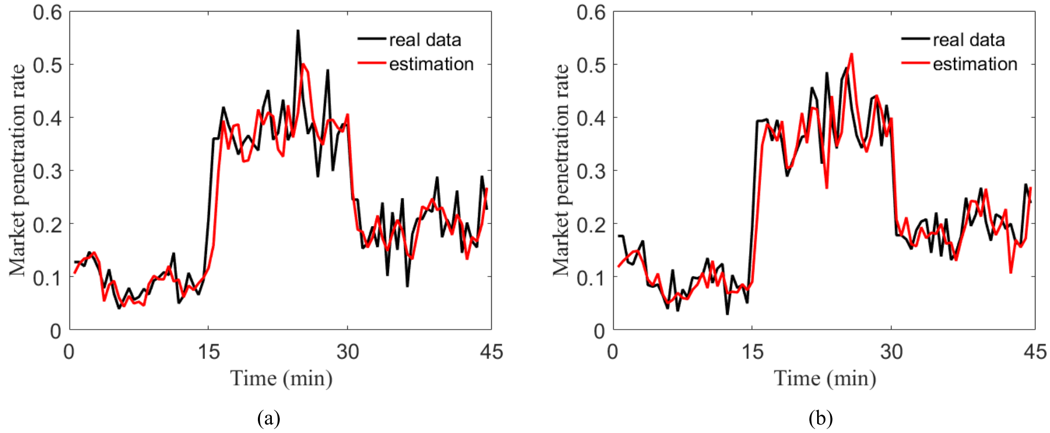

Fig. 11. MPR estimates in Method 3 over a period of 45 minutes with the MPR set to be 10%, 40%, and 20% over the first, second, and third period of 15 minutes: (a) segment 2; (b) segment 3.

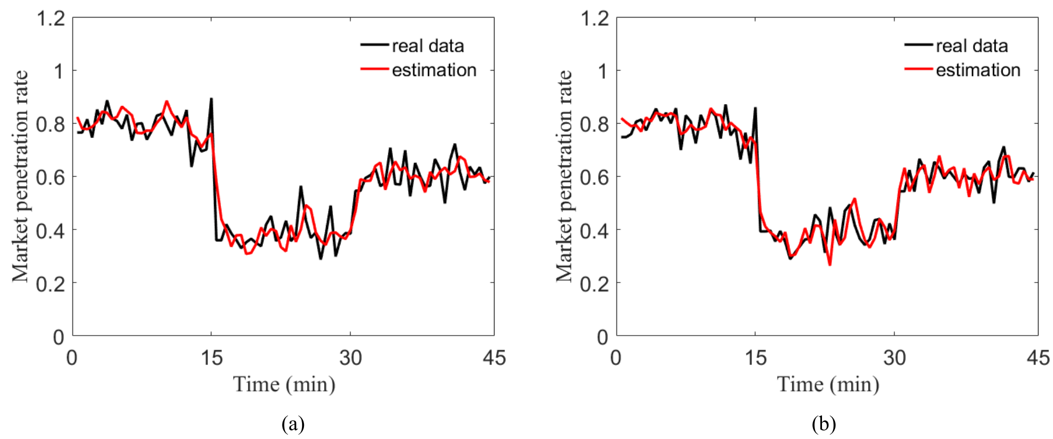

Fig. 12. MPR estimates in Method 3 over a period of 45 minutes with the MPR set to be 40%, 80%, and 60% over the first, second, and third periods of 15 minutes: (a) segment 2; (b) segment 3.

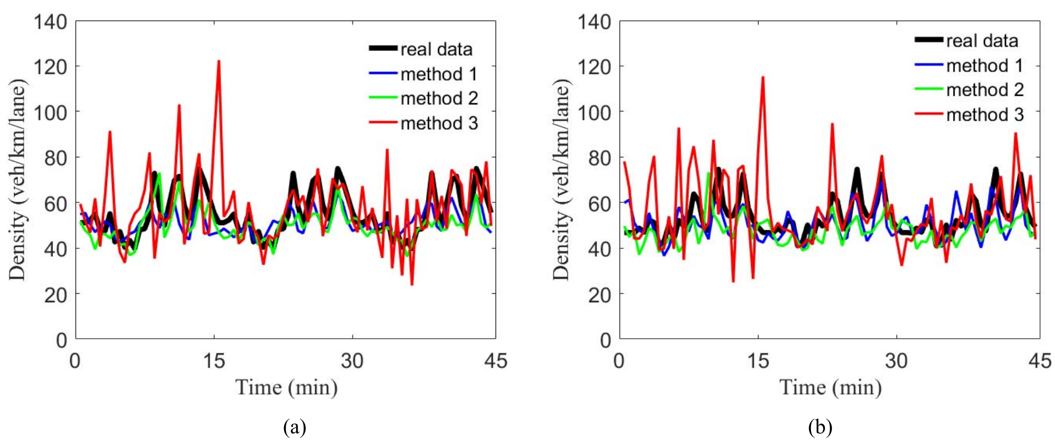

Fig. 13. Segment density estimates corresponding to the MPR scenario in Fig. 11: (a) segment 2; (b) segment 3.

(3) when MPR is bigger than 50%, *Method 3* is recommended for density and MPR estimation.

The traffic flow model employed by *Method 1* is more complex than those by *Methods 2* and *3*. The above observations indicate that, when MPR is very low, *Method 1* can better compensate the deficiency in traffic measurements through its comprehensive traffic flow model. With the increase of MPR, however, the richness of mobile sensing data weakens the importance of traffic flow modeling for TSE, and hence allow *Methods 2 and 3* to adopt simpler modeling structures and

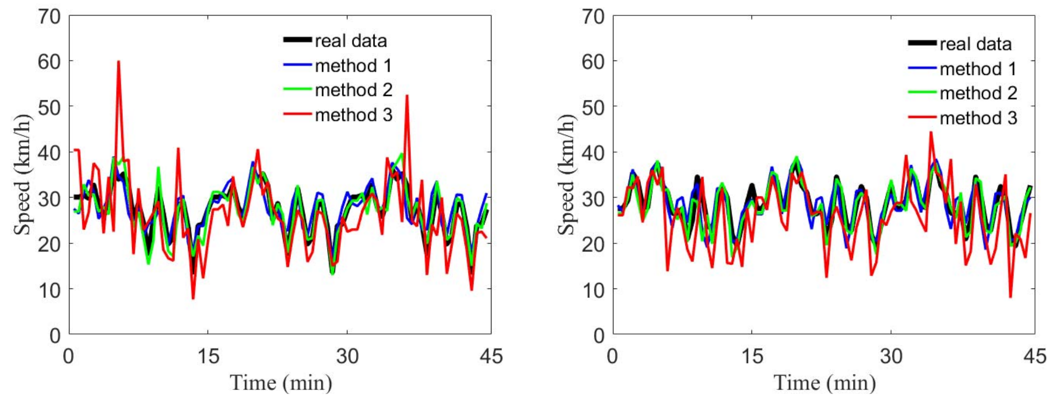

(a) (b)

Fig. 14. Segment speed estimates corresponding to the MPR scenario in Fig. 11: (a) segment 2; (b) segment 3.

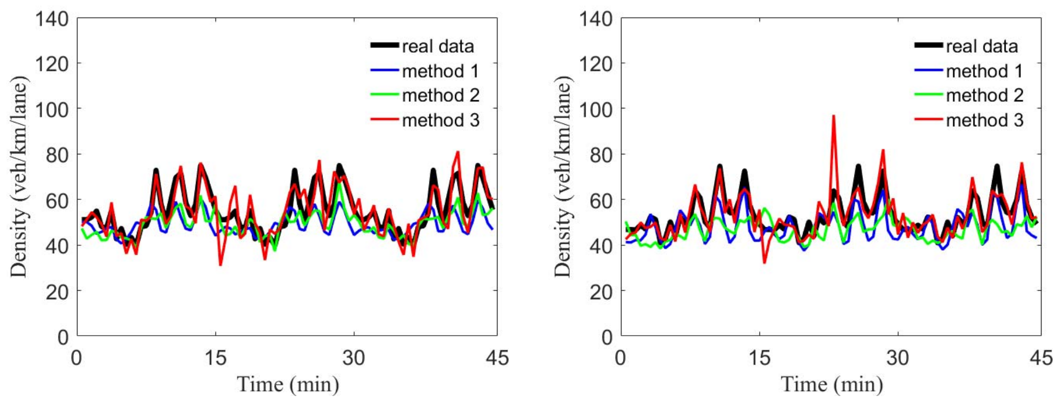

(a) (b)

Fig. 15. Segment density estimates corresponding to the MPR scenario in Fig. 12: (a) segment 2; (b) segment 3.

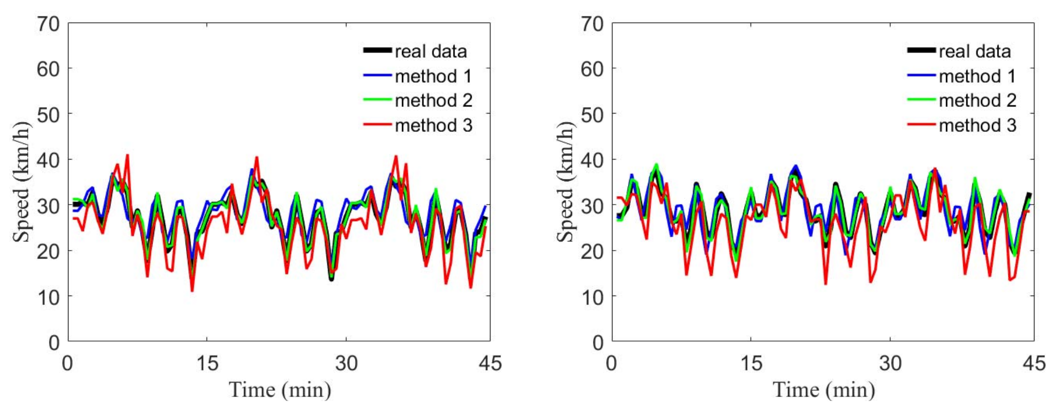

(a) (b)

Fig. 16. Segment speed estimates corresponding to the MPR scenario in Fig. 12: (a) segment 2; (b) segment 3.

also excel in density, speed and MPR estimation. In addition, when MPR ranges between 10% and 50%, *Method 1* may still be recommended for density and MPR estimation, but *Method 2* could be applied instead, if the difference in the estimation accuracy between the two methods is not a major concern (Figs. 4b and 17b). This is because the design and implementation of traffic state estimator in *Method 1* are quite more complex than *Method 2*, due to an extra cost paid to online model parameter estimation (OMPE).

B. Remarks on OMPE

The significance of OMPE for *Method 1* was demonstrated using fixed sensing data [1]–[6], and also confirmed recently with mixed sensing [27]. All results of *Method 1* presented

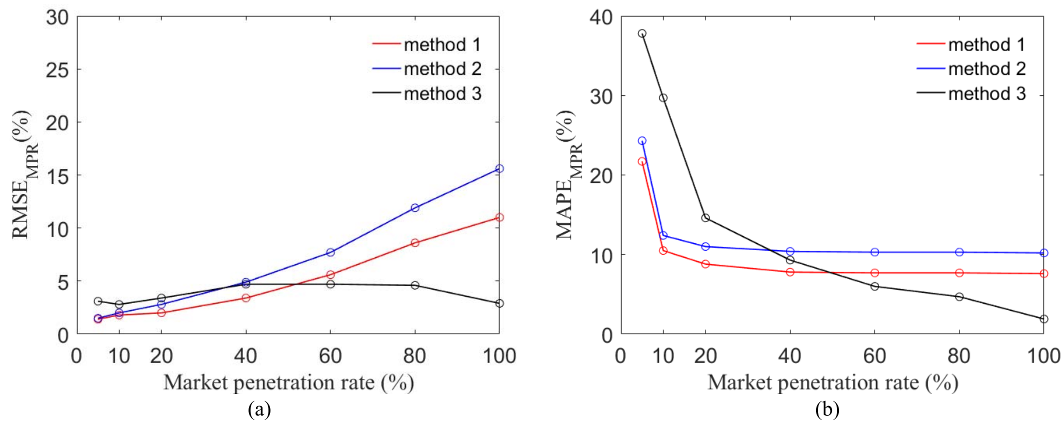

Fig. 17. The comparison of MPR estimation performance for the three methods: (a) RMSE; (b) MAPE.

in this paper already take OMPE into account. *Method 1* was originally developed to work with fixed and sparse sensing data, so it highly relies on comprehensive traffic flow models and OMPE to compensate the shortage of traffic measurements. *Methods 2 and 3*, on the other hand, have been specially designed to operate with mobile sensing data (in addition to a small amount of fixed sensing data for flow observability). The advantages of mobile sensing allow *Methods 2 and 3* to adopt simpler modeling structures that do not need OMPE. On the other hand, the density estimation accuracy of *Method 1* is higher than that of *Method 2* (Fig. 4), and the speed estimation accuracy of *Method 1* is higher than that of *Method 3* (Fig. 5), at the cost of OMPE that involves an empirical and time-consuming process for fine tuning. The interested reader is referred to [27] for more details of OMPE for *Method 1* in the mixed sensing case.

V. CONCLUSION

Three model-based approaches to freeway traffic state estimation have been studied and evaluated in depth using mixed sensing data extracted from the NGSIM data set. The three approaches were carefully compared in terms of their traffic state estimator designs, operating principles, data requirements, and capabilities of estimating traffic flow variables and MPRs of connected vehicles. A few recommendations are given about the choice of methods with the gradual increase of MPR of connected vehicles.

REFERENCES

[1] Y. Wang and M. Papageorgiou, "Real-time freeway traffic state estimation based on extended Kalman filter: A general approach," *Transp. Res. B, Methodol.*, vol. 39, no. 2, pp. 141–167, 2005.

[2] Y. Wang, M. Papageorgiou, and A. Messmer, "RENAISSANCE—A unified macroscopic model-based approach to real-time freeway network traffic surveillance," *Transp. Res. C, Emerg. Technol.*, vol. 14, no. 3, pp. 190–212, Jun. 2006.

[3] Y. Wang, M. Papageorgiou, and A. Messmer, "Real-time freeway traffic state estimation based on extended Kalman filter: A case study," *Transp. Sci.*, vol. 41, no. 2, pp. 167–181, May 2007.

[4] Y. Wang, M. Papageorgiou, and A. Messmer, "Real-time freeway traffic state estimation based on extended Kalman filter: Adaptive capabilities and real data testing," *Transp. Res. A, Policy Pract.*, vol. 42, no. 10, pp. 1340–1358, Dec. 2008.

[5] Y. Wang, M. Papageorgiou, A. Messmer, P. Coppola, A. Tzimitsi, and A. Nuzzolo, "An adaptive freeway traffic state estimator," *Automatica*, vol. 45, no. 1, pp. 10–24, Jan. 2009.

[6] Y. Wang, P. Coppola, A. Tzimitsi, A. Messmer, M. Papageorgiou, and A. Nuzzolo, "Real-time freeway network traffic surveillance: Large-scale field-testing results in southern Italy," *IEEE Trans. Intell. Transp. Syst.*, vol. 12, no. 2, pp. 548–562, Jun. 2011.

[7] T. Seo, A. M. Bayen, T. Kusakabe, and Y. Asakura, "Traffic state estimation on highway: A comprehensive survey," *Annu. Rev. Control*, vol. 43, pp. 128–151, Jan. 2017.

[8] J. C. Herrera and A. M. Bayen, "Incorporation of Lagrangian measurements in freeway traffic state estimation," *Transp. Res. B, Methodol.*, vol. 44, no. 4, pp. 460–481, May 2010.

[9] C. Roncoli, N. Bekiaris-Liberis, and M. Papageorgiou, "Use of speed measurements for highway traffic state estimation: Case studies on NGSIM data and highway A20, Netherlands," *Transp. Res. Rec.*, vol. 2559, no. 1, pp. 90–100, Jan. 2016.

[10] N. Bekiaris-Liberis, C. Roncoli, and M. Papageorgiou, "Highway traffic state estimation with mixed connected and conventional vehicles," *IEEE Trans. Intell. Transp. Syst.*, vol. 17, no. 12, pp. 3484–3497, Dec. 2016.

[11] Y. Yuan, J. W. C. van Lint, R. E. Wilson, F. van Wageningen-Kessels, and S. P. Hoogendoorn, "Real-time Lagrangian traffic state estimator for freeways," *IEEE Trans. Intell. Transp. Syst.*, vol. 13, no. 1, pp. 59–70, Mar. 2012.

[12] Y. Yuan, H. V. Lint, F. V. Wageningen-Kessels, and S. Hoogendoorn, "Network-wide traffic state estimation using loop detector and floating car data," *J. Intell. Transp. Syst.*, vol. 18, no. 1, pp. 41–50, 2014.

[13] D. B. Work, O.-P. Tossavainen, S. Blandin, A. M. Bayen, T. Iwuchukwu, and K. Tracton, "An ensemble Kalman filtering approach to highway traffic estimation using GPS enabled mobile devices," in *Proc. 47th IEEE Conf. Decis. Control*, Cancun, Mexico, Dec. 2008, pp. 5062–5068.

[14] D. B. Work, S. Blandin, O. P. Tossavainen, B. Piccoli, and A. M. Bayen, "A traffic model for velocity data assimilation," *Appl. Math. Res. Exp.*, vol. 2010, no. 1, pp. 1–35, Apr. 2010.

[15] R. Wang, S. Fan, and D. B. Work, "Efficient multiple model particle filtering for joint traffic state estimation and incident detection," *Transp. Res. C, Emerg. Technol.*, vol. 71, pp. 521–537, Oct. 2016.

[16] R. Wang, D. B. Work, and R. Sowers, "Multiple model particle filter for traffic estimation and incident detection," *IEEE Trans. Intell. Transp. Syst.*, vol. 17, no. 12, pp. 3461–3470, Dec. 2016.

[17] J. W. C. van Lint and S. P. Hoogendoorn, "A robust and efficient method for fusing heterogeneous data from traffic sensors on freeways," *Comput. Aided Civil Infrastruct. Eng.*, vol. 25, no. 8, pp. 596–612, Nov. 2010.

[18] M. Treiber, A. Kesting, and R. E. Wilson, "Reconstructing the traffic state by fusion of heterogeneous data," *Comput. Aided Civil Infrastruct. Eng.*, vol. 26, no. 6, pp. 408–419, Aug. 2011.

[19] H. J. Payne, "Models of freeway traffic and control," *Simul. Council Ser.*, vol. 1, no. 1, pp. 51–61, 1971.

[20] G. B. Whitham, *Linear and Nonlinear Waves*. Hoboken, NJ, USA: Wiley, 1974.

[21] A. Aw and M. Rascle, "Resurrection of 'second order' models of traffic flow," *SIAM J. Appl. Math.*, vol. 60, no. 3, pp. 916–938, Jan. 2000.

[22] H. M. Zhang, "A non-equilibrium traffic model devoid of gas-like behavior," *Transp. Res. B, Methodol.*, vol. 36, no. 3, pp. 275–290, 2002.

[23] C. Nanthawichit, T. Nakatsuji, and H. Suzuki, "Application of probe-vehicle data for real-time traffic-state estimation and short-term travel-time prediction on a freeway," *Transp. Res. Rec.*, vol. 1855, no. 1, pp. 49–59, 2003.

[24] Y. Liu, S. He, B. Ran, and Y. Cheng, "A progressive extended Kalman filter method for freeway traffic state estimation integrating multi-source data," *Wireless Commun. Mobile Comput.*, vol. 2018, pp. 1–10, May 2018.

[25] T. Seo and A. M. Bayen, "Traffic state estimation method with efficient data fusion based on the Aw-Rascle-Zhang model," in *Proc. IEEE 20th Int. Conf. Intell. Transp. Syst. (ITSC)*, Yokohama, Japan, Oct. 2017, pp. 1–6.

[26] R. Wang, Y. Li, and D. B. Work, "Comparing traffic state estimators for mixed human and automated traffic flows," *Transp. Res. C, Emerg. Technol.*, vol. 78, pp. 95–110, May 2017.

[27] Y. Wang, M. Zhao, X. Yu, Y. Hu, and J. Guo, "Real-time joint traffic state and model parameter estimation on freeways with fixed sensors and connected vehicles: State-of-the-art overview, methods, and case studies," *Transp. Res. C, Emerg. Technol.*

[28] N. Bekiaris-Liberis, C. Roncoli, and M. Papageorgiou, "Highway traffic state estimation per lane in the presence of connected vehicles," *Transp. Res. B, Methodol.*, vol. 106, pp. 1–28, Dec. 2017.

[29] M. Fountoulakis, N. Bekiaris-Liberis, C. Roncoli, I. Papamichail, and M. Papageorgiou, "Highway traffic state estimation with mixed connected and conventional vehicles: Microscopic simulation-based testing," *Transp. Res. C, Emerg. Technol.*, vol. 78, pp. 13–33, May 2017.

[30] S. Papadopoulou, C. Roncoli, N. Bekiaris-Liberis, I. Papamichail, and M. Papageorgiou, "Microscopic simulation-based validation of a per-lane traffic state estimation scheme for highways with connected vehicles," *Transp. Res. C, Emerg. Technol.*, vol. 86, pp. 441–452, Jan. 2018.

[31] M. Papageorgiou, J.-M. Blosseville, and H. Hadj-Salem, "Macroscopic modelling of traffic flow on the boulevard Périphérique in Paris," *Transp. Res. B, Methodol.*, vol. 23, no. 1, pp. 29–47, Feb. 1989.

[32] A. Messmer and M. Papageorgiou, "METANET: A macroscopic simulation program for motorway networks," *Traffic Eng. Control*, vol. 32, pp. 466–470, Jan. 1990.

[33] M. Kontorinaki, A. Spiliopoulou, C. Roncoli, and M. Papageorgiou, "First-order traffic flow models incorporating capacity drop: Overview and real-data validation," *Transp. Res. B, Methodol.*, vol. 106, pp. 52–75, Dec. 2017.

[34] W. Wong, S. Shen, Y. Zhao, and H. X. Liu, "On the estimation of connected vehicle penetration rate based on single-source connected vehicle data," *Transp. Res. B, Methodol.*, vol. 126, pp. 169–191, Aug. 2019.

[35] G. Comert, "Queue length estimation from probe vehicles at isolated intersections: Estimators for primary parameters," *Eur. J. Oper. Res.*, vol. 252, no. 2, pp. 502–521, Jul. 2016.

[36] C. N. Van Phu and N. Farhi, "Estimation of urban traffic state with probe vehicles," *IEEE Trans. Intell. Transp. Syst.*, vol. 22, no. 5, pp. 2797–2808, May 2021.

[37] N. Zhou, D. Meng, Z. Huang, and G. Welch, "Dynamic state estimation of a synchronous machine using PMU data: A comparative study," *IEEE Trans. Smart Grid*, vol. 6, no. 1, pp. 450–460, Jan. 2015.

[38] A. Farina, B. Ristic, and D. Benvenuti, "Tracking a ballistic target: Comparison of several nonlinear filters," *IEEE Trans. Aerosp. Electron. Syst.*, vol. 38, no. 3, pp. 854–867, Jul. 2002.

[39] J. Kim, S. S. Vaddi, P. K. Menon, and E. J. Ohlmeyer, "Comparison between nonlinear filtering techniques for spiraling ballistic missile state estimation," *IEEE Trans. Aerosp. Electron. Syst.*, vol. 48, no. 1, pp. 313–328, Jan. 2012.

[40] T Yuan, Y. Bar-Shalom, P. Willett, R. Ben-Dov, and S. Pollak, "A comparison of multiple-IMM estimation approaches using EKF, UKF, and PF for impact point prediction," *Proc. SPIE*, vol. 9092, Jun. 2014, Art. no. 90920D.

[41] I. R. Petersen and A. V. Savkin, *Robust Kalman Filtering for Signals and Systems With Large Uncertainties*. Boston, MA, USA: Birkhauser, 1999.

[42] V. Punzo, M. T. Borzacchiello, and B. Ciuffo, "On the assessment of vehicle trajectory data accuracy and application to the next generation simulation (NGSIM) program data," *Transp. Res. C, Emerg. Technol.*, vol. 19, pp. 1243–1262, Dec. 2011.

[43] M. Marcello and V. Punzo, "Making NGSIM data usable for studies on traffic flow theory: Multistep method for vehicle trajectory reconstruction," *Transp. Res. Rec., J. Transp. Res. Board*, vol. 2390, pp. 99–111, Dec. 2013.

[44] M. Montanino and V. Punzo, "Reconstructed NGSIM I80-1," Cost Action TU0903-Multitude, Eur. Commission's Program COST, Tech. Rep., 2013. [Online]. Available: http://www.multitude-project.eu/exchange/101.html

Mingming Zhao received the B.S. degree in traffic engineering from Northwestern Polytechnical University, China, in 2015. She is currently pursuing the Ph.D. degree with the Institute of Intelligent Transportation Systems, Zhejiang University, China. Her research interests include traffic flow modeling, freeway traffic state estimation, connected and automated vehicles, and intelligent transportation systems.

Claudio Roncoli received the Ph.D. degree in system monitoring and environmental risk management from the University of Genova, Italy, in 2013. He is currently an Assistant Professor of transportation engineering at Aalto University, Finland. Before joining Aalto University, he was a Research Assistant at the University of Genova from 2007 to 2013, a Visiting Research Assistant at Imperial College London, U.K., from 2011 to 2012, and a Post-Doctoral Research Associate at the Technical University of Crete, Greece, from 2013 to 2016. He is the author of more than 90 articles published in international peer-reviewed journals, conference proceedings, and contributed books. His research interests include real-time traffic management, modeling, optimization, and control of traffic systems with connected and automated vehicles, as well as smart mobility and intelligent transportation systems. He has been involved in several national and international research projects, also as a Principal Investigator. He is a scientific committee member of several major international conferences. He is an Associate Editor for *IET Intelligent Transport Systems* journal and the *Proceedings of the Institution of Civil Engineers—Transport*. He is an Editorial Advisory Board Member for *Transportation Research Part C: Emerging Technologies*. He regularly acts as a Reviewer for high-impact journals in the field, including IEEE TRANSACTIONS ON INTELLIGENT TRANSPORTATION SYSTEMS, *Transportation Research Part C: Emerging Technologies*, and *Transportation Research Part B: Methodological*.

Yibing Wang (Member, IEEE) received the B.Sc. degree in electronics and computer engineering from Sichuan University, Chengdu, China, the M.Eng. degree in automatic control engineering from Chongqing University, Chongqing, China, and the Ph.D. degree in control theory and applications from Tsinghua University, Beijing, China. He was a Post-Doctoral Researcher/Research Fellow/Senior Research Fellow with the Dynamic Systems and Simulation Laboratory, Department of Production Engineering and Management, Technical University of Crete, Greece, from 1999 to 2007. He was a Senior Lecturer at the Department of Civil Engineering, Monash University, Australia, from 2007 to 2013. Since 2013, he has been a Full Professor with the Institute of Intelligent Transportation Systems, Zhejiang University, China. His research interests include road traffic flow modeling, traffic surveillance, urban and freeway traffic control, and connected and automated vehicles (CAV). His research has been supported by the European Commission, the Discovery Program of the Australian Research Council, the National Natural Science Foundation of China, the National Key Research and Development Program of China, and the Provincial Key Research and Development Program of Zhejiang. He and his few students were the recipients of the First Best Conference Paper Award at the 23rd IEEE International Conference on Intelligent Transportation Systems in 2020. He serves as a Senior Editor for IEEE TRANSACTIONS ON INTELLIGENT TRANSPORTATION SYSTEMS and an Associate Editor for *Transportation Research Part C: Emerging Technologies*.

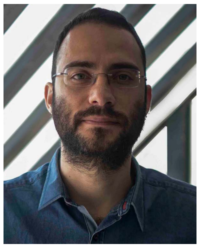

Nikolaos Bekiaris-Liberis (Member, IEEE) received the Ph.D. degree in aerospace engineering from the University of California, San Diego, USA, in 2013. From 2013 to 2014, he was a Post-Doctoral Researcher with the University of California, Berkeley, USA. From 2017 to 2019, he was a Marie Sklodowska-Curie Fellow and from 2014 to 2017, he was a Research Associate at the Technical University of Crete, Greece. He is currently an Assistant Professor with the Department of Electrical and Computer Engineering, Technical University of Crete. He has authored/coauthored one book and more than 100 papers. His interests include nonlinear delay, switched, and distributed parameter systems and their applications to transport systems. He received the Chancellor's Dissertation Medal in Engineering from the University of California, San Diego, in 2014. He was a recipient of the 2016 Marie Sklodowska-Curie Individual Fellowship Grant. He serves as an Associate Editor for *Automatica* and IEEE TRANSACTIONS ON INTELLIGENT TRANSPORTATION SYSTEMS.

Jingqiu Guo received the B.Sc. degree in computer science from Southeast University, China, the Post-graduate Diploma degree in informatics from Vrije Universiteit Brussel, Belgium, and the Ph.D. degree in transportation economics from The University of Western Australia (UWA) in 2012. She was with the Transport and Logistic Centre, UWA, Australia. She is currently an Associate Professor with Tongji University, China. Her research interests include driving behavior modeling and vehicular *ad-hoc* networks.

Senlin Cheng received the B.Eng. degree in measurement technology and instrument and the Ph.D. degree in mechanical manufacturing and automation from Chongqing University, Chongqing, China, in 1990 and 1999, respectively. He is currently an Associate Professor with the School of Automation, Chongqing University. His research interests include vehicle lane perception and intelligent driving.